

Chapter 6

Gas-Phase Photochemistry

Chemical reactions in the atmosphere result largely from the absorption of solar radiation in the visible and ultraviolet spectral regions provided the incoming photons (light quanta) carry sufficient energy for chemical processes to be initiated. Photochemical reactions always occur in two steps: the first is the excitation of a molecule by the absorption of radiation; the second is a reaction of the excited molecule. In atmospheric chemistry, the most important process to be considered is dissociation of the excited molecule. Other modes of energy dissipation, such as fluorescence or collisional energy transfer, usually do not lead to chemical changes so that they are of lesser interest. Any quantitative assessment of the photochemical activity of an atmospheric constituent requires knowledge of (a) the photon flux of solar radiation, (b) the absorption cross section of the species under consideration, and (c) the primary quantum yield of the photo-dissociation process. These parameters depend on the wavelength of radiation; absorption cross sections and quantum yields may additionally depend on temperature and/or pressure.

6.1 Solar Radiation

Solar radiation originates from the very thin outer layers of the sun that (with increasing distance from the center) are designated photosphere, chromosphere and corona. The spectrum consists of a continuum with superimposed line structure. It extends from the soft x-ray region at wavelengths $\lambda < 10$ nm to the far infrared at wavelengths $\lambda > 100$ μm with an intensity maximum occurring in the visible region. At wavelengths beyond about 350 nm the spectrum is that of blackbody at $\sim 5,770$ K, slightly modified by narrow absorption lines (Fraunhofer lines). At shorter wavelengths the solar flux decreases more strongly and, at the shortest wavelengths, departs significantly from that predicted by the blackbody curve. In addition, emission lines become more prominent. The strongest one is the hydrogen Lyman-alpha line at 121.6 nm.

As described in Table 6.1, the extent of attenuation in the terrestrial atmosphere divides the ultraviolet spectrum into characteristic wavelength intervals. In the lower atmosphere solar radiation becomes increasingly scattered. Both Rayleigh scattering by air molecules and Mie scattering by atmospheric particles are important, with Mie scattering occurring mainly in the troposphere. The degree of scattering increases with solar zenith angle (because of increasing slant path length) and with decreasing wavelength ($\sigma_{sc} \propto \lambda^{-n}$, with $n=4$ for Rayleigh scattering and $n=0.5-2.5$ for Mie scattering). In addition, radiation is reflected from Earth's surface. Accordingly, a volume of air receives radiation from all directions. This so-called actinic flux (because it would be determined by a chemical actinometer) must be considered when photochemical processes are involved. In the stratosphere the actinic flux is dominated by direct radiation. In the lower troposphere more than 50% of the actinic flux is due to diffuse sky radiation. Whereas the attenuation of radiation by absorption can be reasonably well calculated and the reflected radiation is determined by the albedo of the ground surface, an assessment of diffuse sky radiation caused by multiple scattering processes requires complex calculation procedures based on radiative transfer models.

The solar flux outside Earth's atmosphere is subject to natural variations, especially in the far ultraviolet spectral region where the variability increases with decreasing wavelength (for details see Chap. 10). Variations in the visible region of the solar spectral irradiance are essentially negligible. However, the eccentricity of Earth's orbit around the sun modulates all wavelength regions equally at $\pm 3.3\%$.

Solar intensities presented in this Section cover the wavelength region 200–870 nm. Data in the far UV at wavelengths below 200 nm are treated in Chap. 10.

Table 6.1 Origin of solar emissions and regions of Earth's atmosphere thereby affected^a

Wavelength range (nm)	Source region	Variation over 11 year cycle	Atmospheric absorption region (principal absorbers)
750–50,000 (IR)	Photosphere		Entire atmosphere (CO ₂ , H ₂ O, O ₃)
400–750 (visible)		0.08%	Entire atmosphere (O ₃ , Chappuis band)
300–400 (UV)		0.1%	Troposphere (O ₃ , NO ₂ , HCHO, others)
200–300 (UV)		0.5–4%	Stratosphere (O ₂ , O ₃ Hartley band)
175–200 (UV)	Upper photosphere	15%	Mesosphere (O ₂ , SRB)
120–175 (far UV)	Chromosphere	50%	Thermosphere (O ₂ , SC)
Lyman- α , 121.6		2 fold	Mesosphere (O ₂ , H ₂ O, NO ionization)
20–120 (EUV)	Transition region ^b	2–10 fold	Thermosphere (N ₂ , O ₂ , O ionization)
0–20 (X-rays)	Corona	10–10 ³ fold	Mesosphere (N ₂ , O ₂ ionization)

^a Adapted from Lean (1991). Abbreviations: IR infrared, UV ultraviolet, EUV extreme ultraviolet, SC Schumann continuum, SRB Schumann-Runge bands

^b The transition region is the region between chromosphere and corona

Table 6.2 Solar radiation intensities at wavelengths from 180 to 400 nm in 1 nm intervals^a

λ_c (nm)	I_{av}	λ_c (nm)	I_{av}	λ_c (nm)	I_{av}	λ_c (nm)	I_{av}	λ_c (nm)	I_{av}
180.5	0.172	226.5	4.651	272.5	28.040	318.5	110.36	364.5	192.48
181.5	0.211	227.5	4.733	273.5	28.005	319.5	118.30	365.5	219.51
182.5	0.213	228.5	6.186	274.5	18.973	320.5	134.48	366.5	235.42
183.5	0.215	229.5	5.706	275.5	25.144	321.5	117.21	367.5	226.07
184.5	0.199	230.5	6.261	276.5	34.993	322.5	115.74	368.5	211.48
185.5	0.223	231.5	6.150	277.5	33.807	323.5	111.49	369.5	236.05
186.5	0.262	232.5	6.454	278.5	23.119	324.5	128.66	370.5	219.90
187.5	0.294	233.5	5.445	279.5	12.462	325.5	148.57	371.5	227.41
188.5	0.323	234.5	4.762	280.5	13.834	326.5	166.67	372.5	204.59
189.5	0.352	235.5	6.311	281.5	30.553	327.5	162.61	373.5	179.11
190.5	0.374	236.5	5.989	282.5	43.304	328.5	157.09	374.5	175.73
191.5	0.416	237.5	5.996	283.5	46.312	329.5	182.13	375.5	207.75
192.5	0.413	238.5	5.216	284.5	34.889	330.5	175.03	376.5	212.85
193.5	0.384	239.5	5.508	285.5	24.275	331.5	166.83	377.5	252.18
194.5	0.528	240.5	4.958	286.5	48.186	332.5	165.48	378.5	261.80
195.5	0.553	241.5	6.479	287.5	50.395	333.5	160.18	379.5	210.91
196.5	0.615	242.5	8.923	288.5	48.450	334.5	167.16	380.5	238.29
197.5	0.637	243.5	8.443	289.5	71.324	335.5	164.94	381.5	215.10
198.5	0.640	244.5	7.769	290.5	91.035	336.5	141.96	382.5	157.74
199.5	0.693	245.5	6.319	291.5	88.237	337.5	148.07	383.5	136.72
200.5	0.765	246.5	6.475	292.5	79.558	338.5	162.57	384.5	192.30
201.5	0.843	247.5	7.159	293.5	81.913	339.5	169.52	385.5	202.60
202.5	0.872	248.5	5.912	294.5	78.086	340.5	178.61	386.5	202.74
203.5	0.978	249.5	7.331	295.5	85.194	341.5	164.42	387.5	202.68
204.5	1.092	250.5	7.846	296.5	78.750	342.5	177.25	388.5	199.29
205.5	1.129	251.5	6.030	297.5	78.657	343.5	170.17	389.5	238.24
206.5	1.192	252.5	5.467	298.5	72.414	344.5	142.85	390.5	253.79
207.5	1.368	253.5	6.811	299.5	75.552	345.5	169.11	391.5	273.75
208.5	1.635	254.5	7.913	300.5	65.774	346.5	167.28	392.5	208.46
209.5	2.334	255.5	10.554	301.5	71.579	347.5	163.30	393.5	119.41
210.5	3.062	256.5	13.610	302.5	77.085	348.5	162.95	394.5	210.91
211.5	3.697	257.5	16.826	303.5	98.165	349.5	162.08	395.5	270.78
212.5	3.466	258.5	16.852	304.5	95.606	350.5	191.80	396.5	176.57
213.5	3.689	259.5	14.069	305.5	94.705	351.5	179.43	397.5	192.40
214.5	4.475	260.5	11.608	306.5	88.766	352.5	166.79	398.5	316.16
215.5	4.060	261.5	12.237	307.5	98.561	353.5	190.24	399.5	346.32
216.5	3.641	262.5	14.179	308.5	98.306	354.5	205.23	400.5	351.01
217.5	4.000	263.5	22.763	309.5	80.084	355.5	193.64	401.5	365.43
218.5	5.052	264.5	34.420	310.5	100.71	356.5	121.96	402.5	368.98
219.5	5.367	265.5	34.964	311.5	118.38	357.5	148.31	403.5	354.05
220.5	5.439	266.5	34.640	312.5	106.82	358.5	129.58	404.5	352.89
221.5	4.568	267.5	34.958	313.5	114.36	359.5	185.68	405.5	352.33
222.5	5.757	268.5	34.116	314.5	108.66	360.5	182.39	406.5	336.63
223.5	7.339	269.5	33.551	315.5	104.08	361.5	165.44	407.5	345.66
224.5	6.900	270.5	37.679	316.5	104.44	362.5	188.51	408.5	369.34
225.5	6.145	271.5	31.750	317.5	128.06	363.5	188.85	409.5	365.91

^aWavelengths λ_c at interval centers; irradiances in units of 10^{12} (photon $\text{cm}^{-2} \text{s}^{-1} \text{nm}^{-1}$) (converted from originally ($\text{mW m}^{-2} \text{nm}^{-1}$)); Upper Atmosphere Research Satellite data validated by Spacelab ATLAS 2 measurements in April 1993. Source: Woods et al. (1996)

Table 6.3 Comparison of solar flux measurements in the near ultraviolet spectral region averaged over 5 nm intervals (units: 10^{12} photon cm^{-2} s^{-1} nm^{-1})^a

$\Delta\lambda$ (nm)	A	B	C	D	E	F	G	H
	Nov	July	May	Dec	Dec	Aug	Mar	Apr
	1978	1980	1982	1983	1984	1985	1992	1993
180–185	0.16	0.19	0.17	–	0.17	–	0.22	0.20
185–190	0.24	0.27	0.24	–	0.26	–	0.31	0.29
190–195	0.36	0.39	0.40	–	0.41	–	0.44	0.42
195–200	0.57	0.59	0.61	–	0.63	–	0.66	0.63
200–205	0.80	0.87	0.84	0.82	0.94	0.94	0.95	0.91
205–210	1.37	1.45	1.39	1.45	1.59	1.53	1.59	1.53
210–215	3.28	3.52	3.36	3.27	3.83	3.56	3.73	3.68
215–220	3.98	4.42	4.06	4.35	4.52	4.26	4.48	4.42
220–225	5.54	6.19	5.74	5.74	6.56	5.72	6.05	6.00
225–230	4.94	5.60	5.45	5.12	5.83	5.04	5.53	5.48
230–235	5.23	5.93	5.42	5.43	5.92	5.28	5.86	5.81
235–240	5.16	5.93	5.67	5.46	5.93	5.46	5.85	5.80
240–245	6.79	7.07	7.35	6.98	7.22	7.10	7.35	7.31
245–250	5.95	6.42	6.49	6.32	6.69	6.48	6.70	6.64
250–255	6.13	6.61	6.64	6.40	6.95	6.61	6.89	6.81
255–260	12.9	13.8	14.3	13.8	14.7	13.9	14.5	14.4
260–265	17.7	19.0	19.4	19.6	20.3	19.5	19.0	19.0
265–270	32.3	32.7	34.2	35.9	36.1	35.3	34.7	34.4
270–275	27.5	27.5	28.7	30.2	30.1	30.3	29.1	28.9
275–280	25.2	25.4	26.6	27.4	26.8	26.9	26.2	25.9
280–285	32.0	33.3	34.5	37.4	36.2	37.2	34.1	33.8
285–290	46.5	47.6	50.8	53.7	54.1	52.4	48.5	48.5
290–295	84.0	79.8	84.5	88.2	88.4	87.8	83.8	83.8
295–300	74.8	73.0	78.1	81.4	80.4	82.0	77.9	78.1
300–305	82.3	73.6	77.8	89.7	90.1	84.6	82.1	81.6
305–310	94.1	81.9	87.5	100.3	97.1	101.2	92.6	92.1
310–315	112	95.6	99.1	116.6	119.8	120.0	109.8	109.8
315–320	112	–	–	119.1	–	120.4	113.1	113.1
320–325	119	–	–	126.6	–	131.0	121.5	121.5
325–330	165	–	–	171.6	–	170.6	163.4	163.4
330–335	159	–	–	171.4	–	168.4	166.9	166.9
335–340	159	–	–	163.3	–	162.8	157.5	157.5

^aA: Nimbus 7 satellite solar UV backscatter measurements, reconstructed from data reported by Simon (1981) and Mentall et al. (1981), originally Heath (1980, unpublished); B: Rocket flight July 15, 1980, near solar maximum, Mount and Rottman (1983); C: Rocket flight May 17, 1982, Mount and Rottman (1983); D: Spacelab 1 (Space Shuttle Columbia) November–December 1983, Labs et al. (1987); E: Rocket flight December 1984, Mentall and Williams (1988); F: Spacelab 2 (Space Shuttle Challenger) August 1985, VanHoosier et al. (1988) as reported by Nicolet (1989); G, H: Upper Atmosphere Research Satellite validated by Space Shuttle ATLAS 1 and 2 measurements in March 1992 (near solar maximum) and April 1993, respectively, Woods et al. (1996). (ATLAS Atmospheric Laboratory for Applications and Science)

Table 6.4a Solar radiation intensities at wavelengths from 330 to 630 nm in 1 nm intervals^a

λ_c (nm)	+0.0	+1.0	+2.0	+3.0	+4.0	+5.0	+6.0	+7.0	+8.0	+9.0
330.5	167.5	161.7	154.3	152.1	158.4	166.0	129.8	147.3	156.3	160.3
340.5	170.2	161.1	171.7	170.5	124.9	168.4	160.5	158.0	166.5	152.4
350.5	197.8	175.9	154.7	198.8	202.6	189.5	168.5	160.5	113.3	206.0
360.5	177.9	162.9	214.8	175.5	186.4	232.8	230.8	225.0	202.2	248.0
370.5	200.9	244.8	199.9	157.8	165.7	216.1	209.1	245.7	255.9	191.2
380.5	247.3	210.9	141.3	132.2	199.0	185.3	208.6	188.6	178.6	241.0
390.5	240.8	275.9	188.9	97.1	219.1	274.8	129.9	208.3	308.9	333.2
400.5	332.9	363.6	365.9	337.2	326.6	341.7	332.7	317.4	375.7	352.1
410.5	310.8	377.4	372.5	366.4	363.3	363.5	387.3	350.8	355.6	360.1
420.5	373.0	382.4	337.3	365.6	378.7	363.9	365.4	338.5	343.2	319.8
430.5	246.6	367.1	359.2	378.6	366.2	378.6	425.0	398.9	346.8	404.9
440.5	380.7	430.3	442.2	427.3	442.6	409.5	426.2	469.0	446.6	459.8
450.5	487.4	480.5	443.3	450.9	453.9	467.6	478.5	484.8	456.1	465.9
460.5	474.1	478.6	491.0	477.2	463.2	479.7	452.3	475.4	471.5	471.5
470.5	445.8	480.2	486.7	475.8	491.1	482.8	470.4	500.0	485.1	502.3
480.5	493.5	507.8	492.6	492.6	481.5	448.5	399.0	450.3	471.9	484.2
490.5	496.8	470.4	471.3	470.3	513.6	481.7	505.4	506.7	469.5	496.6
500.5	469.1	458.7	480.4	491.5	475.9	508.4	501.3	488.2	492.5	492.7
510.5	501.6	515.5	483.0	482.4	486.7	494.4	435.0	450.7	432.8	479.4
520.5	481.1	501.7	480.8	500.5	518.3	511.9	444.7	486.8	506.0	512.6
530.5	522.6	526.6	475.8	517.8	501.3	537.8	506.7	510.6	517.5	498.9
540.5	482.7	514.1	499.8	515.5	516.4	523.4	518.3	506.6	515.8	525.6
550.5	517.4	520.8	514.8	525.8	531.2	531.9	511.5	519.5	503.8	510.6
560.5	521.4	517.0	525.3	529.3	528.3	513.3	523.0	540.5	519.4	534.7
570.5	509.5	525.9	546.7	543.1	541.4	531.6	537.2	541.3	520.7	534.7
580.5	538.6	543.9	550.7	546.9	548.8	527.0	541.8	548.0	519.6	479.6
590.5	540.4	533.6	540.8	538.1	532.1	533.0	543.5	536.9	530.9	536.9
600.5	529.0	531.4	522.6	544.4	542.0	538.9	538.6	538.9	535.2	536.3
610.5	524.6	538.7	526.9	521.0	531.1	532.0	500.6	531.9	538.0	533.6
620.5	542.9	530.0	538.1	524.2	521.9	515.2	536.5	537.3	538.2	532.7

^aWavelengths λ_c at interval centers; irradiances in units of 10^{12} (photon $\text{cm}^{-2} \text{s}^{-1} \text{nm}^{-1}$) (converted from originally ($\mu\text{W cm}^{-2} \text{\AA}^{-1}$)); Source: Neckel and Labs (1984)

Table 6.4b Solar radiation intensities at wavelengths from 630 to 870 nm in 2 nm intervals^a

λ_c (nm)	I_{av}	λ_c (nm)	I_{av}	λ_c (nm)	I_{av}	λ_c (nm)	I_{av}	λ_c (nm)	I_{av}
631.0	521.9	679.0	513.4	727.0	493.7	775.0	464.7	823.0	445.8
633.0	527.4	681.0	512.9	729.0	485.2	777.0	469.0	825.0	447.7
635.0	530.6	683.0	509.9	731.0	489.1	779.0	466.7	827.0	449.2
637.0	531.7	685.0	503.1	733.0	487.5	781.0	467.9	829.0	448.6
639.0	532.4	687.0	508.7	735.0	485.4	783.0	464.7	831.0	447.6
641.0	522.1	689.0	508.1	737.0	486.0	785.0	467.5	833.0	434.0
643.0	526.0	691.0	505.1	739.0	476.6	787.0	467.5	835.0	443.0
645.0	529.6	693.0	506.6	741.0	470.4	789.0	467.5	837.0	443.7
647.0	523.4	695.0	503.8	743.0	482.1	791.0	462.3	839.0	440.5
649.0	510.3	697.0	498.2	745.0	480.8	793.0	457.5	841.0	442.8
651.0	527.6	699.0	502.8	747.0	483.6	795.0	455.0	843.0	436.7
653.0	527.0	701.0	490.5	749.0	480.0	797.0	463.4	845.0	439.8
655.0	506.5	703.0	492.6	751.0	478.2	799.0	457.7	847.0	437.5
657.0	459.1	705.0	503.6	753.0	478.4	801.0	461.7	849.0	415.4
659.0	515.2	707.0	499.7	755.0	478.1	803.0	457.6	851.0	430.1
661.0	524.1	709.0	495.4	757.0	476.7	805.0	453.1	853.0	418.2
663.0	520.3	711.0	497.2	759.0	474.9	807.0	456.2	855.0	377.9
665.0	523.6	713.0	494.3	761.0	475.0	809.0	447.2	857.0	436.6
667.0	516.8	715.0	493.1	763.0	477.8	811.0	456.0	859.0	431.6
669.0	522.0	717.0	489.8	765.0	471.4	813.0	457.6	861.0	432.6
671.0	513.4	719.0	481.8	767.0	458.7	815.0	455.4	863.0	434.4
673.0	516.7	721.0	484.2	769.0	466.9	817.0	455.3	865.0	422.8
675.0	514.5	723.0	491.7	771.0	468.5	819.0	439.5	867.0	384.5
677.0	515.3	725.0	493.8	773.0	471.2	821.0	447.6	869.0	423.5

^a Wavelengths λ_c at interval centers, irradiances in units of 10^{12} (photon $\text{cm}^{-2} \text{s}^{-1} \text{nm}^{-1}$) (originally ($\mu\text{W cm}^{-2} \text{\AA}^{-1}$)); Source: Neckel and Labs (1984)

Comments: Center-of-disc spectral intensities were measured at the Jungfraujoeh (Swiss Alps, 3,600 m a.s.l.) and corrected for (wavelength-dependent) limb darkening and telluric absorptions. These data have served as a standard for many years despite indications by some other studies that at wavelengths <500 nm the intensities are slightly too low. Recent measurements have confirmed this effect (see the following Table 6.5 for a comparison).

Table 6.5 Comparison of solar irradiances measured in the wavelength range 330–670 nm^a

$\Delta\lambda$ (nm)	A	B	C	$\Delta\lambda$ (nm)	A	B	C
	Intensity ^a				Intensity ^a		
330–335	158.8	162.7	–	500–505	475.1	481.4	485.4
335–340	151.9	160.2	–	505–510	496.6	501.3	511.5
340–345	159.7	170.3	–	510–515	493.8	493.0	492.8
345–350	161.1	169.9	174.1	515–520	458.4	459.5	459.5
350–355	186.0	197.0	193.1	520–525	496.5	502.1	494.2
355–360	203.1	178.0	193.9	525–530	492.4	497.4	490.5
360–365	183.5	194.9	197.4	530–535	508.8	513.1	512.9
365–370	227.7	242.5	236.1	535–540	514.3	518.2	512.4
370–375	193.8	206.7	215.5	540–545	505.7	510.7	512.0
375–380	223.6	241.4	231.8	545–550	517.9	520.1	522.0
380–385	186.1	197.0	188.4	550–555	522.0	523.2	527.7
385–390	200.4	212.2	211.2	555–560	515.5	513.9	516.9
390–395	204.4	215.0	216.6	560–565	524.3	519.9	515.2
395–400	251.0	263.3	209.6	565–570	526.2	523.1	517.8
400–405	345.3	359.9	375.2	570–575	533.3	530.9	527.2
405–410	343.9	358.8	355.2	575–580	533.1	528.2	527.7
410–415	358.1	373.4	359.2	580–585	545.8	538.1	539.5
415–420	463.5	381.3	372.2	585–590	523.2	517.9	524.0
420–425	367.4	384.1	378.6	590–595	537.0	532.1	530.6
425–430	346.1	358.3	360.3	595–600	536.2	532.4	536.1
430–435	343.5	357.1	341.9	600–605	533.9	527.8	532.3
435–440	390.8	404.1	395.6	605–610	537.6	528.8	534.3
440–445	424.6	438.6	435.7	610–615	528.5	516.8	524.5
445–450	442.2	454.8	450.3	615–620	527.2	514.2	517.9
450–455	463.2	475.4	466.5	620–625	531.9	516.4	527.2
455–460	470.6	480.2	486.4	625–630	532.0	516.5	530.3
460–465	476.8	486.8	491.4	630–635	525.8	510.4	526.1
465–470	470.1	481.5	483.5	635–640	531.8	515.7	530.0
470–475	475.9	483.6	492.8	640–645	525.2	509.7	523.2
475–480	488.1	496.4	510.7	645–650	519.4	504.6	521.2
480–485	493.6	504.7	508.6	650–655	523.1	514.4	525.7
485–490	450.8	461.6	466.9	655–660	491.0	478.3	486.4
490–495	484.5	493.6	497.9	660–665	522.5	510.9	520.4
495–500	492.0	498.6	498.0	665–670	520.2	508.1	518.6

^aAveraged intensities in 5 nm intervals: Units: 10^{12} (photon $\text{cm}^{-2} \text{s}^{-1} \text{nm}^{-1}$). A: Neckel and Labs (1984), Ground-based measurements at the Jungfrauoch (Swiss Alps, 3,600 m a.s.l.); B: Burlov-Vasiljev et al. (1995), ground-based measurements at the high altitude observatory at Terskol Peak (Caucasus, 3,100 m a.s.l.), data presented in 5 nm intervals; C: Thuillier et al. (1998) Observations from Space Shuttle Atlantis (ATLAS 1 mission) in March 1992, 1 nm intervals (approximately)

References

- Burlov-Vasiljev, K.A., A. Gurtovenko, Y.B. Matvejev, *Solar Phys.* **157**, 51–73 (1995)
- Labs, D., H. Neckel, P.C. Simon, G. Thuillier, *Solar Phys.* **107**, 203–219 (1987)
- Lean, J., *Rev. Geophys.* **29**, 505–535 (1991)
- Mentall, J.E., D.E. Williams, *J. Geophys. Res.* **93**, 735–746 (1988)
- Mentall, J.E., J.E. Frederick, J.R. Herman, *J. Geophys. Res.* **86**, 9881–9884 (1981)
- Mount, G.H., G.J. Rottman, *J. Geophys. Res.* **88**, 5403–5410, 6807–6811 (1983)
- Neckel, H., D. Labs, *Solar Phys.* **90**, 205–258 (1984)
- Nicolet, M., *Planet. Space Sci.* **37**, 1249–1289 (1989)
- Simon, P.C., *Solar Phys.* **74**, 273–291 (1981)
- Thuillier, G., M. Hersé, P.C. Simon, D. Labs, H. Mandel, D. Gillotay, T. Foujols, *Solar Phys.* **177**, 41–61 (1998)
- VanHoosier, M.E., J.-D.F. Bratov, G.E. Brueckner, D.K. Prinz, *Astrophys. Lett. Comm.* **27**, 163–168 (1988)
- Woods, T.N., D.K. Prinz, G.J. Rottman, J. London, P.C. Crane, R.P. Cebula, E. Hilsenrath, G.E. Brueckner, M.D. Andrews, O.R. White, M.E. VanHoosier, L.E. Floyd, L.C. Herring, B.G. Knapp, C.K. Pankratz, P.A. Reiser, *J. Geophys. Res.* **101** D6, 9541–9569 (1996)

6.2 Photodissociation Coefficients

The absorption cross section (σ_s) is defined by the Beer-Lambert law written in the form

$$\sigma_s(\lambda) = (1/n_s l) \ln(I_0(\lambda)/I_t(\lambda))$$

where l is the absorption path length, n_s is the number concentration of the absorbing species s assumed to be constant along the absorption path, and $I_0(\lambda)$ and $I_t(\lambda)$ are the incident and transmitted light intensities at wavelength λ , respectively. The units adopted for the absorption cross section: ($\text{cm}^2 \text{ molecule}^{-1}$) are associated with the units for number concentration (molecule cm^{-3}) and path length (cm). Owing to space limitations, the unit for absorption cross sections often is simplified to (cm^2) (with the entity omitted).

The primary quantum yield of a photochemical process is the probability of a molecule to enter into a specific chemical reaction following excitation by absorption of a photon. The dissociation quantum yield ϕ_i ($\text{molecule photon}^{-1}$) is the probability for decomposition of the excited molecule along a specific product channel i . Other possible primary processes such as isomerization, fluorescence or collisional energy transfer must be assigned the corresponding quantum yields. The sum of quantum yields for all primary processes is equal to unity. This follows directly from the energy balance. Discrete band spectra indicate transitions to bound upper energy levels that may or may not undergo predissociation by interacting with another unstable state. Conversely, a continuous spectrum usually indicates a transition to an unstable, that is dissociating, upper state. If this is the only allowed photodissociation process, the dissociation quantum yield is close to unity.

These quantities are combined with the actinic radiation flux to derive photodissociation coefficients for atmospheric constituents. The photodissociation coefficient, j , (sometimes called the photodissociation frequency) is defined by the integral over the effective wavelength region

$$j_i = \int_{\Delta\lambda} \phi_1(\lambda) \sigma_s(\lambda) I_a(\lambda) d\lambda \quad [\text{s}^{-1}]$$

where ϕ_1 is the associated primary quantum yield, $\sigma_s(\lambda)$ is the absorption cross section of the dissociating molecule, and $I_a(\lambda)$ is the actinic radiation flux, with units ($\text{photon cm}^{-2} \text{s}^{-1} \text{nm}^{-1}$) if $\sigma_s(\lambda)$ is given in ($\text{cm}^2 \text{molecule}^{-1}$). The photodissociation rate $-dn_s/dt$ ($\text{molecule cm}^{-3} \text{s}^{-1}$) refers to the loss of photo-active species n_s . The rate of product formation must take the stoichiometry of the process into account. For example, the rate of OH formation associated with the process $\text{H}_2\text{O}_2 + h\nu \rightarrow \text{OH} + \text{OH}$ is $dn_{\text{OH}}/dt = -2dn_{\text{H}_2\text{O}_2}/dt = 2j_{\text{H}_2\text{O}_2} n_{\text{H}_2\text{O}_2}$.

Table 6.6 presents an overview of absorption spectra and photochemical processes in the atmosphere. Individual data are treated subsequently.

Table 6.6 Overview on absorption spectra and photochemical products of gas-phase atmospheric constituents and their significance to atmospheric chemistry^a

Constituent	Absorption spectrum		Photochemistry		Quantum yield	Significance in the atmosphere
	Type and approximate long wavelength limit (nm)	Dissociation limit (nm)	Main primary photochemical process	Photochemistry		
N ₂	Lyman-Birge-Hopfield bands	145	127	Predissociation		Not significant, the absorption is too weak
O ₂	Herzberg bands	275				Night-sky emission, high altitude
	Herzberg continuum	240	240	O ₂ → O(³ P) + O(³ P)	φ ≈ 1.0	O ₃ formation in the stratosphere
	Schumann-Runge bands	200		Predissociation	φ ≈ 1.0	Important in the mesosphere
O ₃	Schumann continuum	175	175	O ₂ → O(³ P) + O(¹ D)	φ ≈ 1.0	O ₂ dissociation in upper atmosphere
	Hartley bands	320	310	O ₃ → O ₂ (¹ Δ _{g) + O(¹D)}	φ ≈ 0.9	Important in the stratosphere
	Huggins bands	360	410	O ₃ → O ₂ (³ Σ _g ⁻) + O(³ P)	φ ≈ 1.0	Important in the troposphere
	Chappuis bands	850	1,180	O ₃ → O ₂ (³ Σ _g ⁻) + O(³ P)	φ ≈ 1.0	Entire atmosphere
	Continuum overlapped by bands	200	226	(a) CO ₂ → CO + O(³ P) (b) CO ₂ → CO + O(¹ D)	φ ≈ 1.0	(a) Mesosphere and stratosphere, 175–200 nm; (b) shielded by O ₂
CO	4th positive band system	155	167	Fluorescence-quenching		Not significant
CH ₄	Continuum, some band structure	160	277	Dissociation		Not significant, shielded by O ₂
H ₂	Lyman bands	111	275	Fluorescence-quenching	φ ≈ 1.0	Not significant
H ₂ O	Continuum, some band structure	200	243	H ₂ O → OH + H	Small	Mesosphere and stratosphere, 175–200 nm
	Continuum	350	557	H ₂ O → H ₂ + O (¹ D) H ₂ O → OH + OH H ₂ O → HO ₂ + H	φ ≈ 1.0	Stratosphere and mesosphere
HO ₂	Continuum	270	437	HO ₂ → O + HO (presumably)		Possibly in the mesosphere
N ₂ O	Continuum, some band structure	240	742	(a) N ₂ O → N ₂ + O (³ P)	Spin-forbidden	Stratosphere > 185 nm
	Bands + continuum	235	341	(b) N ₂ O → N ₂ + O (¹ D)	φ ≈ 1.0	Not significant
NH ₃			281	Dissociation		

NO	Resonance bands Continuum + bands	230	191	(a) Predissociation, mainly the bands 0-0 and 0-1	(a) Mesosphere and upper stratosphere
NO ₂	Complex band system	135	134	(b) Photoionization	(b) Lyman α , upper mesosphere
		700	398	(a) NO ₂ \rightarrow NO + O (³ P)	(a) Very important throughout the entire atmosphere
NO ₃	Continuum < 250 nm Diffuse bands	690	244	(b) NO ₂ \rightarrow NO + O (¹ D)	(b) Possibly in the mesosphere
		395	587	NO ₃ \rightarrow NO ₂ + O	Important
HONO	Diffuse bands	330	1,139	NO ₃ \rightarrow NO + O ₂	586 < λ < 640 nm
		410	578	HNO ₂ \rightarrow NO + OH	Important in the entire atmosphere
HNO ₃	Continuum	330	361	HNO ₂ \rightarrow H + NO ₂	Mainly in the stratosphere
		410	604	HNO ₃ \rightarrow NO ₂ + OH	
N ₂ O ₅	Continuum	330	1,252	N ₂ O ₅ \rightarrow NO ₂ + NO ₃	Stratosphere
		370	298	N ₂ O ₅ \rightarrow NO ₃ + NO + O	
HO ₂ NO ₂	Continuum, bands	220	1,191	HO ₂ NO ₂ \rightarrow HO ₂ + NO ₂	Entire atmosphere
		277	731	HO ₂ NO ₂ \rightarrow OH + NO ₃	
Cl ₂	Continuum	220	493	Cl ₂ \rightarrow Cl + Cl	Possibly in the mesosphere, > 175 nm
		420	277	HCl \rightarrow H + Cl	
HOCl	Continuum	220	500	HOCl \rightarrow OH + Cl	Entire atmosphere
		300	347	CH ₃ Cl \rightarrow CH ₃ + Cl	
CH ₃ Br	Continuum	370	417	CH ₃ Br \rightarrow CH ₃ + Br	Stratosphere
		103	501	CH ₃ I \rightarrow CH ₃ + I	
CF ₄	Continuum, bands	230	220	CF ₄ \rightarrow CF ₃ + F (presumably)	Not competitive
		220	375	CFCl ₃ \rightarrow CFCl ₂ + Cl	
CF ₂ Cl ₂	Continuum	240	354	CFCl ₃ \rightarrow CFCl ₂ + Cl	Important
		240	407	CF ₂ Cl ₂ \rightarrow CF ₂ Cl + Cl	
CCl ₄	Continuum	240	407	CF ₂ Cl ₂ \rightarrow CFCl + 2Cl	Important in the stratosphere, in the O ₂ absorption window
		240	407	CCl ₄ \rightarrow CCl ₃ + Cl	
				CCl ₄ \rightarrow CCl ₂ + 2Cl	Important in the stratosphere in the O ₂ absorption window

(continued)

Table 6.6 (continued)

Constituent	Absorption spectrum		Photochemistry		Quantum yield	Significance in the atmosphere
	Type and approximate long wavelength limit (nm)	Dissociation limit (nm)	Main primary photochemical process			
HF	Continuum	211	HF → H + F			Shielded by O ₂
ClONO ₂	Continuum	162	ClONO ₂ → Cl + NO ₃		0.4 < φ < 1.0	Stratosphere
	Continuum	430	ClONO ₂ → ClO + NO ₂		0 < φ < 0.6	
			ClONO ₂ → ClONO + O		φ = 0.17 (at λ = 220 nm)	
ClONO	Continuum	400	ClONO → Cl + NO ₂ (expected)			Not established
Cl ₂	Continuum	470	Cl ₂ → Cl + Cl		φ ≈ 1	Entire atmosphere
ClOOCl	Continuum	450	ClOOCl → ClOO + Cl		φ ≈ 1	Polar stratosphere
PAN ^b	Continuum	350	PAN → CH ₃ CO ₃ + NO ₂		φ ≈ 0.75	Significance not established
			PAN → CH ₃ CO ₂ + NO ₃		φ ≈ 0.25	
C ₂ -C ₅ alkanes	Continuum	170	Photodecomposition			Not significant
C ₂ -C ₅ alkenes	Continuum	205	Photodecomposition			Not significant
C ₂ H ₂	Continuum, weak structure	237	C ₂ H ₂ → C ₂ H + H			Significance not established
HCHO	Bands	360	HCHO → H + HCO		φ depends on λ and p	Important in the entire atmosphere
			HCHO → H ₂ + CO			
CH ₃ CHO	Quasi-continuum, weak structure	340	CH ₃ CHO → CH ₃ + CHO		φ depends on λ and p	Significant in the troposphere
	Quasi-continuum, weak structure	350	CH ₃ CO CH ₃ → CH ₃ CO + CH ₃		φ depends on λ and p	

CH ₃ OOH	Continuum	350	647	CH ₃ OOH → CH ₃ O + OH	φ ≈ 1.0	Possibly stratosphere
SO ₂	Very weak bands,	390		Excited state quenching and reaction		Not significant because of collisional quenching
	Stronger bands	340				
OCS	Continuum + bands	220	220	SO ₂ → SO + O		Stratosphere
	Continuum	300	388	OCS → CO + S(³ P)	φ ≈ 0.27	Stratosphere
			286	OCS → CO + S(¹ D)	φ ≈ 0.67	
CH ₃ SH	Continuum	280	311	CH ₃ SH → CH ₃ S + H	φ ≈ 0.9	Not significant
CS ₂	Two strongly	370	281	CS ₂ → CS + S(³ P)		Not significant
	structured bands		223	CS ₂ → CS + S(¹ D)		Not significant
CH ₃ SSCH ₃	Continuum	355	437	CH ₃ SSCH ₃ → 2 CH ₃ S	φ = 1.65 (at λ = 248 nm)	Significant in the troposphere

^aSource of data: Warneck (2000), with changes and additions (with permission of Elsevier)

^bPAN = peroxyacetyl nitrate, CH₃C(O)OONO₂

Table 6.7 Photodissociation coefficients for important atmospheric processes^a

Reaction	$\lambda_{\text{threshold}}$ or $\Delta\lambda$ (nm)	Ground level	25 km altitude
		Photolysis frequency (s^{-1})	
$\text{O}_2 + h\nu \rightarrow \text{O} (^3\text{P}) + \text{O} (^3\text{P})$	245	4.3 (-26)	1.2 (-11)
$\text{O}_3 + h\nu \rightarrow \text{O}_2 + \text{O} (^3\text{P})$	310–850	4.2 (-4)	5.0 (-4)
$\text{O}_3 + h\nu \rightarrow \text{O}_2 (\text{a } ^1\Delta_{\text{g}}) + \text{O} (^1\text{D})$	310	5.1 (-5)	1.1 (-4)
$\text{H}_2\text{O} + h\nu \rightarrow \text{H} + \text{OH}$	210	0	6.6 (-11)
$\text{H}_2\text{O}_2 + h\nu \rightarrow \text{OH} + \text{OH}$	355	7.7 (-6)	1.2 (-5)
$\text{CH}_3\text{OOH} + h\nu \rightarrow \text{CH}_3\text{O} + \text{OH}$	360	5.7 (-6)	9.9 (-6)
$\text{NO}_2 + h\nu \rightarrow \text{NO} + \text{O} (^3\text{P})$	420	8.8 (-3)	1.2 (-2)
$\text{NO}_3 + h\nu \rightarrow \text{NO}_2 + \text{O} (^3\text{P})$	410–640	2.8 (-1)	3.0 (-1)
$\text{NO}_3 + h\nu \rightarrow \text{NO} + \text{O}_2$	586–640	2.5 (-2)	2.7 (-2)
$\text{N}_2\text{O}_5 + h\nu \rightarrow \text{NO}_2 + \text{NO}_3$	385	5.0 (-5)	4.7 (-5)
$\text{N}_2\text{O} + h\nu \rightarrow \text{N}_2 + \text{O} (^1\text{D})$	240	1.8 (-23)	2.5 (-8)
$\text{HONO} + h\nu \rightarrow \text{NO} + \text{OH}$	400	1.9 (-3)	2.8 (-3)
$\text{HNO}_3 + h\nu \rightarrow \text{NO}_2 + \text{OH}$	335	8.2 (-7)	5.6 (-6)
$\text{HO}_2\text{NO}_2 + h\nu \rightarrow \text{HO}_2 + \text{NO}_2$	330	3.7 (-6)	1.1 (-5)
$\text{HO}_2\text{NO}_2 + h\nu \rightarrow \text{OH} + \text{NO}_3$	334	1.8 (-6)	5.7 (-6)
$\text{HCHO} + h\nu \rightarrow \text{H}_2 + \text{CO}$	360	4.4 (-5)	7.6 (-5)
$\text{HCHO} + h\nu \rightarrow \text{H} + \text{HCO}$	340	3.3 (-5)	6.2 (-5)
$\text{CH}_3\text{CHO} + h\nu \rightarrow \text{CH}_3 + \text{HCO}$	325	6.4 (-6)	1.3 (-5)
$\text{CH}_3\text{COCH}_3 + h\nu \rightarrow \text{CH}_3 + \text{CH}_3\text{CO}$	335	8.4 (-7)	1.9 (-6)
$\text{CH}_3\text{COCHO} + h\nu \rightarrow \text{CH}_3\text{CO} + \text{CO} + \text{H}$	465	2.9 (-4)	3.8 (-4)
$\text{CH}_3\text{ONO}_2 + h\nu \rightarrow \text{CH}_3\text{O} + \text{NO}_2$	330	1.3 (-6)	2.5 (-6)
$\text{C}_2\text{H}_5\text{ONO}_2 + h\nu \rightarrow \text{C}_2\text{H}_5\text{O} + \text{NO}_2$	330	1.8 (-6)	1.5 (-5)
$\text{C}_3\text{H}_7\text{ONO}_2 + h\nu \rightarrow \text{C}_3\text{H}_7\text{O} + \text{NO}_2$	330	3.4 (-6)	1.9 (-5)
$\text{CH}_3\text{OONO}_2 + h\nu \rightarrow \text{CH}_3\text{O}_2 + \text{NO}_2$	325	6.4 (-6)	1.8 (-5)
$\text{CH}_3\text{CO}_3\text{NO}_2 + h\nu \rightarrow \text{CH}_3\text{CO}_3 + \text{NO}_2$	300	7.2 (-8)	3.5 (-6)
$\text{CH}_3\text{SSCH}_3 + h\nu \rightarrow \text{CH}_3\text{S} + \text{CH}_3\text{S}$	400	6.3 (-5)	1.3 (-4)
$\text{COS} + h\nu \rightarrow \text{CO} + \text{S}$	260	1.7 (-21)	2.8 (-8)
$\text{Cl}_2 + h\nu \rightarrow \text{Cl} + \text{Cl}$	450	2.4 (-3)	3.5 (-3)
$\text{ClO} + h\nu \rightarrow \text{Cl} + \text{O}$	305	4.1 (-5)	1.3 (-4)
$\text{ClO} + h\nu \rightarrow \text{ClO} + \text{O}$	450	9.9 (-2)	1.4 (-1)
$\text{ClOOCl} + h\nu \rightarrow \text{ClOO} + \text{Cl}$	360	1.2 (-3)	2.0 (-3)
$\text{HOCl} + h\nu \rightarrow \text{Cl} + \text{OH}$	420	2.6 (-4)	4.1 (-4)
$\text{ClONO}_2 + h\nu \rightarrow \text{Cl} + \text{NO}_3$	400	4.8 (-5)	6.2 (-5)
$\text{ClNO}_2 + h\nu \rightarrow \text{Cl} + \text{NO}_2$	372	3.9 (-4)	6.5 (-4)
$\text{CCl}_4 + h\nu \rightarrow \text{CCl}_3 + \text{Cl}$	250	2.1 (-21)	8.5 (-7)
$\text{CFCl}_3 + h\nu \rightarrow \text{CFCl}_2 + \text{Cl}$	250	4.3 (-22)	5.1 (-7)
$\text{CF}_2\text{Cl}_2 + h\nu \rightarrow \text{CF}_2\text{Cl} + \text{Cl}$	226	1.7 (-23)	4.6 (-8)
$\text{CFCl}_2\text{CF}_2\text{Cl} + h\nu \rightarrow \text{CF}_2\text{ClCF}_2 + \text{Cl}$	230	2.6 (-23)	8.8 (-8)
$\text{CH}_3\text{Cl} + h\nu \rightarrow \text{CH}_3 + \text{Cl}$	220	2.3 (-24)	1.3 (-8)
$\text{CH}_3\text{CCl}_3 + h\nu \rightarrow \text{Cl} + \text{products}$	240	5.1 (-23)	7.2 (-7)
$\text{CHF}_2\text{Cl} + h\nu \rightarrow \text{Cl} + \text{products}$	205	3.0 (-27)	5.7 (-10)
$\text{Br}_2 + h\nu \rightarrow \text{Br} + \text{Br}$	600	3.0 (-2)	3.6 (-2)
$\text{BrCl} + h\nu \rightarrow \text{Br} + \text{Cl}$	570	4.6 (-3)	5.9 (-3)
$\text{HOBr} + h\nu \rightarrow \text{Br} + \text{OH}$	480	6.1 (-4)	9.1 (-4)
$\text{BrO} + h\nu \rightarrow \text{Br} + \text{O}$	375	3.8 (-3)	5.9 (-3)
$\text{BrONO}_2 + h\nu \rightarrow \text{Br} + \text{NO}_3$	390	1.1 (-3)	1.6 (-3)
$\text{CH}_3\text{Br} + h\nu \rightarrow \text{Br} + \text{CH}_3$	260	4.0 (-21)	1.1 (-6)
$\text{CH}_3\text{I} + h\nu \rightarrow \text{I} + \text{CH}_3$	365	1.4 (-6)	2.5 (-5)

^aPowers of ten in parentheses; calculated with overhead sun, surface albedo 0.03; from the summary of Jacobson (2005), data for CH_3I from Rattigan et al. (1997)

Table 6.8 Stratospheric photodissociation rates (s^{-1}) as a function of altitude^a

Altitude (km)	20	25	30	40	50	60
N ₂ O	3.08 (-9)	2.76 (-8)	1.07 (-7)	3.87 (-7)	6.15 (-7)	7.09 (-7)
CFCl ₃	6.46 (-8)	5.75 (-7)	2.21 (-6)	7.69 (-6)	1.15 (-5)	1.37 (-5)
CF ₂ Cl ₂	4.34 (-9)	4.17 (-8)	1.75 (-7)	7.96 (-7)	1.58 (-6)	2.14 (-6)

^aPowers of ten in parentheses; calculated by Mérienne et al. (1990) for an overhead sun

Table 6.9 Photodissociation coefficients for different wavelength regions^a

Constituent or process	Wavelength region (nm)	j (s^{-1})	Constituent or process	Wavelength region (nm)	j (s^{-1})
O ₃	<310	8.7 (-3)	HO ₂ NO ₂	<300	6.3 (-4)
	>310	4.6 (-4)		>300	1.5 (-4)
CO ₂	Ly α	2.2 (-8)	HCl	>175	1.2 (-6)
	>175	1.9 (-9)		HOCl	<300
H ₂ O	Ly α	4.2 (-6)	CH ₃ Cl	>300	3.7 (-4)
	>175	8.6 (-7)		>175	1.0 (-7)
H ₂ O ₂	<300	1.0 (-4)	CFCl ₃	>175	1.0 (-7)
	>300	1.3 (-5)	CF ₂ Cl ₂	>175	6.3 (-7)
N ₂ O	>175	7.3 (-7)	CCl ₄	>175	3.5 (-5)
NO ₂	175–240	5.9 (-5)	ClO	<300	6.5 (-3)
	240–307	2.3 (-4)		>300	5.5 (-4)
	>310	8.0 (-3)		ClONO ₂	<310
NO ₃ → NO ₂ + O	>400	1 (-1)	ClONO	>310	9.5 (-4)
NO ₃ → NO + O ₂		4 (-2)		<310	2.0 (-5)
N ₂ O ₅	<310	5.8 (-4)		>310	9.5 (-4)
	>310	3.6 (-5)	HCHO → H	<300	4.5 (-5)
HNO ₃	<200	7.1 (-5)	+ HCO	>300	1.1 (-5)
	200–307	7.2 (-5)	HCHO → H ₂	<300	4.0 (-5)
	>307	2.0 (-6)	+ CO	>300	1.1 (-5)
HNO ₂	<310	3.4 (-4)	CH ₃ OOH	>300	1.2 (-5)
	>310	2.5 (-3)			

^aPowers of ten in parentheses; from Warneck (2000) with permission of Elsevier, originally Nicolet (1978) calculated with solar radiation intensities incident on Earth's atmosphere

References

- Jacobson, M.Z., *Fundamentals of Atmospheric Modeling*, 2nd edn. (Cambridge University Press, Cambridge, 2005)
- Mérienne, M.F., B. Coquart, A. Jenouvrier, *Planet. Space Sci.* **38**, 617–625 (1990)
- Nicolet, M., *Etude des réactions chimiques de l'ozone dans la stratosphère* (Institut Royal Météorologique de Belgique, Belgium, 1978)
- Rattigan, O.V., D.E. Shallcross, R.A. Cox, *J. Chem. Soc. Faraday Trans.* **93**, 2839–2846 (1997)
- Warneck, P., *Chemistry of the Natural Atmosphere*, 2nd edn. (Academic Press, San Diego, 2000), Copyright Elsevier

6.3 Absorption Cross Sections and Primary Quantum Yields

Absorption cross sections and quantum yields for many gaseous species of interest in atmospheric chemistry have been critically reviewed by Atkinson et al. (2004, 2006, 2007) and by Sander et al. (2006). These publications have served as a guide in selecting the data presented below. For definitions of absorption cross sections and quantum yields see the introduction to the preceding Sect. 6.2 on photodissociation coefficients.

Table 6.10 Absorption cross sections of molecular oxygen in the Herzberg continuum^a

λ (nm)	$10^{24}\sigma_0$ (cm ²)	$10^{27}\alpha$ (cm ² hPa ⁻¹)	λ (nm)	$10^{24}\sigma_0$ (cm ²)	$10^{27}\alpha$ (cm ² hPa ⁻¹)	λ (nm)	$10^{24}\sigma_0$ (cm ²)	$10^{27}\alpha$ (cm ² hPa ⁻¹)
194.6	1.97	18.2	215	5.36	7.32	229	2.50	3.87
200.8	5.63	12.5	217	4.92	6.83	231	2.13	3.47
205	6.90	10.3	219	4.45	6.40	233	1.98	3.10
207	6.66	9.68	221	4.09	5.78	235	1.67	2.76
209	6.35	9.08	223	3.73	5.22	237	1.24	2.48
211	5.95	8.63	225	3.30	4.72	239	1.01	2.18
213	5.63	8.03	227	2.84	4.37	240	0.92	2.02

^aSource of data: Yoshino et al. (1988, 1992). The absorption cross sections are pressure-dependent: $\sigma(\lambda) = \sigma_0(\lambda) + \alpha(\lambda)P$, where $\alpha(\lambda)$ is a cross section involving two oxygen molecules. Values for $\sigma_0(\lambda)$ and $\alpha(\lambda)$ are presented above

Comments: At wavelength below 200 nm the Herzberg continuum underlies the Schumann-Runge band system and is effective only in windows between rotational lines. In this region the intensity of the Herzberg continuum declines to low values near 190 nm. The quantum yield for the process $O_2 + h\nu \rightarrow 2 O(^3P)$ is $\phi = 1.0$ for the entire wavelength region 175–242 nm. Yoshino et al. (1992) have fitted the observed wavelength dependence of cross sections of the Herzberg continuum to a fourth order polynomial with the following parameters: $y(\lambda \text{ [nm]}) = 10^{24}\sigma_0$, $a_0 = -2.3837947 \times 10^4$, $a_1 = 4.1973085 \times 10^2$, $a_2 = -2.7640139$, $a_3 = 8.0723193 \times 10^{-3}$, $a_4 = 8.8255447 \times 10^{-6}$.

Table 6.11a Absorption cross sections of ozone in the Hartley band^a

λ (nm)	$10^{18} \sigma$ ($\text{cm}^2 \text{ molecule}^{-1}$)		λ (nm)	$10^{20} \sigma$ ($\text{cm}^2 \text{ molecule}^{-1}$)		λ (nm)	$10^{22} \sigma$ ($\text{cm}^2 \text{ molecule}^{-1}$)	
	298 K	226 K		298 K	226 K		298 K	226 K
185	0.6537	0.6437	230	4.476	4.506	275	5.913	5.871
186	0.6187	0.6259	232	5.181	5.230	276	5.450	5.379
188	0.5659	0.5655	234	5.891	5.923	278	4.668	4.617
190	0.5114	0.5163	235	6.318	6.349	280	4.001	3.983
192	0.4606	0.4595	236	6.722	6.772	282	3.250	3.220
194	0.4066	0.4088	238	7.486	7.532	284	2.712	2.644
195	0.3864	0.3827	240	8.314	8.367	285	2.465	2.398
196	0.3673	0.3642	242	8.971	9.016	286	2.238	2.195
198	0.3349	0.3333	244	9.717	9.752	288	1.750	1.687
200	0.3154	0.3145	245	9.932	10.28	290	1.418	1.365
202	0.3179	0.3156	246	10.33	10.42	292	1.111	1.043
204	0.3365	0.3400	248	10.71	10.79	294	0.8711	0.8148
205	0.3385	0.3623	250	11.24	11.34	295	0.7753	0.7270
206	0.3855	0.3887	252	11.55	11.65	296	0.6727	0.6202
208	0.4640	0.4684	254	11.59	11.69	298	0.5124	0.4714
210	0.5716	0.5806	255	11.61	11.45	300	0.3964	0.3616
212	0.7194	0.7312	256	11.54	11.58	301	0.3463	0.3128
214	0.9096	0.9255	258	11.24	11.30	302	0.3073	0.2796
215	1.023	1.041	260	10.80	10.86	303	0.2650	0.2325
216	1.081	1.169	262	10.57	10.64	304	0.2401	0.2156
218	1.439	1.464	264	10.06	10.13	305	0.2015	0.1771
220	1.785	1.799	265	9.657	9.612	306	0.1808	0.1603
222	2.200	2.217	266	9.485	9.467	307	0.1565	0.1367
224	2.684	2.688	268	8.754	8.722	308	0.1364	0.1202
225	2.943	2.963	270	7.980	7.961	309	0.1243	0.1064
226	3.226	3.239	272	7.147	7.107	310	0.1020	0.08637
228	3.829	3.857	274	6.140	6.013	311	0.0926	0.07925

^aThe temperature dependence of cross sections in the Hartley band is slight and shows up mainly in the long wavelength tail. Source of data: Molina and Molina (1986)

Table 6.11b Absorption cross sections of ozone in the wavelength region of the Huggins bands^a

λ (nm)	$10^{20} \sigma$ ($\text{cm}^2 \text{ molecule}^{-1}$)		λ (nm)	$10^{21} \sigma$ ($\text{cm}^2 \text{ molecule}^{-1}$)		λ (nm)	$10^{21} \sigma$ ($\text{cm}^2 \text{ molecule}^{-1}$)	
	295 K	218 K		295 K	218 K		295 K	218 K
312.0	7.868	6.416	322.0 p	2.423	2.158	330.8 v	6.379	4.524
312.5	7.221	5.792	322.5 v	21.70	17.15	331.0	8.406	7.088
313.0	6.712	5.495	322.6 p	24.13	20.98	331.1 p	8.529	7.269
313.5	6.968	5.952	323.0	19.60	14.32	331.5	6.239	4.356
314.0	6.291	5.073	323.5	13.93	8.248	332.0	4.182	2.259
314.5	5.364	4.041	323.9 v	11.77	6.562	332.5 v	3.083	1.433
315.0	5.096	3.973	324.5 s	12.83	8.769	333.0 s	3.416	2.072
315.1	5.015	3.911	324.8 p	18.23	16.43	333.5	4.465	3.240
315.5 p	5.461	4.675	325.0	17.28	14.57	333.7 p	5.888	5.022
316.0	4.664	3.636	325.3 v	14.19	10.47	334.0	5.319	3.785
316.5	4.180	3.141	325.5 p	15.09	12.16	334.5	3.516	2.008
316.8 v	3.907	2.880	326.0	11.06	6.997	335.0	2.391	1.208
317.0 p	4.128	3.317	326.5	8.575	4.677	335.6 s	1.876	8.112
317.4 v	3.910	3.061	326.8 v	7.702	4.087	336.0	1.770	7.504
317.6 p	4.219	3.614	327.0	8.383	5.557	336.5 p	2.702	1.810
318.0	3.699	2.948	327.2 p	9.634	7.280	336.8 v	2.513	1.536
318.5	3.082	2.185	327.5 v	8.839	6.129	337.0	2.072	1.283
319.1 v	2.660	1.836	327.9 p	13.09	11.97	337.3 p	3.855	3.392
319.5 p	3.205	2.644	328.0	12.99	11.40	337.5	3.251	2.597
319.8 v	2.959	2.318	328.5	9.406	5.991	338.0	2.072	1.283
320.0	3.250	2.835	329.0	6.419	3.167	338.5	1.405	0.6684
320.5 s	2.540	1.862	329.4 v	5.137	2.413	339.0 v	1.322	0.5069
321.0	1.996	1.268	329.6 s	5.048	2.528	339.5 p	1.655	0.6423
321.1 v	1.915	1.239	329.9 v	4.637	2.458	339.7 v	1.555	0.6129
321.4 p	1.923	1.322	330.0	4.695	2.634	340.0	2.031	1.403
321.6 v	1.837	1.233	330.3 p	7.376	6.043	340.2 p	2.211	1.667
λ (nm)	$10^{21} \sigma$ ($\text{cm}^2 \text{ molecule}^{-1}$)		λ (nm)	$10^{21} \sigma$ ($\text{cm}^2 \text{ molecule}^{-1}$)		λ (nm)	$10^{21} \sigma$ ($\text{cm}^2 \text{ molecule}^{-1}$)	
	295 K	220 K		295 K	220 K		295 K	220 K
340.5	1.747	1.134	345.0	0.685	0.355	349.1 v	0.231	0.070
341.0	1.095	0.587	345.5	0.606	0.247	349.5 p	0.374	0.102
341.5	0.755	0.325	346.0	0.592	0.184	350.0	0.294	0.080
341.8 v	0.692	0.298	346.5	0.493	0.141	350.5	0.258	0.088
342.0	0.749	0.300	346.7 v	0.440	0.116	350.7 v	0.235	0.084
342.1 p	0.781	0.297	346.9 v	0.408	0.140	350.9 v	0.220	0.088
342.6 v	0.670	0.219	347.0	0.426	0.190	351.0	0.230	0.101
343.0	0.907	0.327	347.2 p	0.518	0.356	351.4 p	0.399	0.321
343.2 p	0.952	0.445	347.5	0.455	0.298	352.0	0.291	0.186
343.5 v	0.882	0.423	348.0	0.316	0.159	352.5	0.295	0.132
344.0 p	1.371	1.179	348.5	0.269	0.103	353.0	0.222	0.081
344.5	0.954	0.683	349.0	0.249	0.074	354.0	0.127	0.042

^aPeaks (p), valleys (v) and shoulders (s) are indicated. Source of data (upper part): Malicet et al. (1995), numerical data were taken from the compilation of Keller-Rudek and Moortgat (2010); (lower part) Cacciani et al. (1989)

Table 6.11c Quantum yields for the process $O_3 + h\nu \rightarrow O_2 + O(^1D)$ at 298 and 223 K^a

λ (nm)	ϕ_{298}	ϕ_{223}	λ (nm)	ϕ_{298}	ϕ_{223}	λ (nm)	ϕ_{298}	ϕ_{223}	λ (nm)	ϕ_{298}	ϕ_{223}
305	0.900	–	311	0.310	0.23	317	0.222	0.08	323	0.113	0.05
306	0.884	0.86	312	0.310	0.16	318	0.206	0.08	324	0.101	0.06
307	0.862	0.84	313	0.265	0.13	319	0.187	0.08	325	0.092	0.08
308	0.793	0.74	314	0.246	0.09	320	0.166	0.07	326	0.086	0.08
309	0.671	0.61	315	0.239	0.09	321	0.146	0.07	327	0.082	0.08
310	0.523	0.39	316	0.233	0.09	322	0.128	0.07	328	0.080	0.07

^aIn the wavelength region $220 < \lambda < 305$ nm, $\phi(O^1D) = 0.90$, $\phi(O^3P) = 0.10$; in the wavelength region $330 < \lambda < 370$, $\phi(O^1D) = 0.08$, $\phi(O^3P) = 0.92$ (independent of temperature in both regions). Source of data: Talukdar et al. (1998)

Matsumi et al. (2002) have proposed the following formula for $O(^1D)$ quantum yields in the wavelength region 306–328 nm:

$$\phi(\lambda, T) = A_1[1/(1+q)]\exp[-(x_1 - \lambda)/\omega_1]^4 + A_2[q/(1+q)](T/300)^2 \\ \times \exp[-(x_2 - \lambda)/\omega_2]^2 + A_3(T/300)^{1.5} \exp[-(x_3 - \lambda)/\omega_3]^2 + C$$

with $q = \exp(-825.518/R_g T)$ and the constants $A_1 = 0.8036$, $A_2 = 8.9061$, $A_3 = 0.1192$, $x_1 = 304.225$, $x_2 = 314.957$, $x_3 = 310.737$, $\omega_1 = 5.576$, $\omega_2 = 6.601$, $\omega_3 = 2.187$, $C = 0.08$.

Table 6.12 Absorption cross sections of ozone in the Chappuis band^a

λ (nm)	$10^{22} \sigma$ (cm ²)	λ (nm)	$10^{22} \sigma$ (cm ²)	λ (nm)	$10^{22} \sigma$ (cm ²)	λ (nm)	$10^{22} \sigma$ (cm ²)	λ (nm)	$10^{22} \sigma$ (cm ²)
377.5*	0.044	490	8.135	590	44.34	680	13.64	800	1.554
390	0.069	500	11.96	595	47.33	690	11.19	810	1.846
395	0.103	510	15.55	600	51.18	700	8.618	815	2.226
400	0.110	520	18.15	603	51.90	710	7.268	820	2.074
410	0.270	530	26.67	605	51.38	720	6.174	825	1.427
420	0.369	540	29.26	610	47.58	730	4.743	830	0.991
430	0.651	550	33.56	620	40.32	740	4.274	838	0.749
440	1.368	560	39.56	630	35.40	750	4.276	853	1.417
450	1.899	570	46.56	640	29.49	760	2.838	877	0.368
460	3.732	575	47.98	650	24.94	770	2.569	898	0.620
470	4.174	580	46.17	660	20.92	780	3.214	933	0.161
480	7.601	585	44.35	670	16.85	790	2.064	944	0.407

^aThe asterisk indicates the minimum of absorption between the visible and near ultraviolet spectral regions. Absorption maxima occur at 575 and 603 nm. The cross sections are independent of temperature. The quantum yield for $O_3 + h\nu \rightarrow O_2(X^3\Sigma_g^-) + O(^3P)$ is unity. Source of data: Brion et al. (1998) (1 nm averages), numerical values taken from the compilation of Keller-Rudek and Moortgat (2010); above 830 nm Anderson et al. (1993) (spectral resolution 3.1 nm)

Table 6.13a Absorption cross sections of nitrogen dioxide, NO₂ (298 K)^a

λ (nm)	$10^{19} \sigma$ (cm ²)	λ (nm)	$10^{19} \sigma$ (cm ²)	λ (nm)	$10^{19} \sigma$ (cm ²)	λ (nm)	$10^{19} \sigma$ (cm ²)	λ (nm)	$10^{19} \sigma$ (cm ²)
205	3.581	295	1.064	385	5.942	475	3.849	565	0.870
210	4.451	300	1.299	390	6.200	480	3.345	570	0.848
215	4.887	305	1.604	395	5.920	485	2.518	575	0.471
220	4.672	310	1.882	400	6.385	490	3.075	580	0.447
225	3.904	315	2.174	405	5.768	495	2.930	585	0.469
230	2.765	320	2.542	410	6.153	500	1.82	590	0.539
235	1.653	325	2.879	415	5.892	505	2.43	595	0.408
240	0.830	330	3.188	420	5.950	510	2.31	600	0.395
245	0.375	335	3.587	425	5.670	515	1.60	605	0.185
250	0.146	340	4.020	430	5.405	520	1.61	610	0.254
255	0.109	345	4.175	435	5.555	525	1.79	615	0.353
260	0.154	350	4.616	440	4.842	530	1.53	620	0.257
265	0.218	355	4.982	445	4.882	535	1.06	625	0.196
270	0.292	360	5.077	450	4.958	540	1.08	630	0.121
275	0.406	365	5.501	455	4.123	545	1.27	635	0.133
280	0.527	370	5.607	460	4.299	550	1.10	640	0.153
285	0.682	375	5.888	465	4.086	555	0.797	645	0.192
290	0.864	380	5.924	470	3.357	560	0.605	650	0.135

^aCross sections represent $\lambda \pm 2.5$ nm averages; the temperature dependence is minimal. Sources of data: Jenouvrier et al. (1996), Mérianne et al. (1995), Vandaele et al. (1998)

Comments: Nitrogen dioxide features a band system with complex structure ranging from ~275 to 900 nm. To display full details requires very high spectral resolution, too detailed for a complete listing of numerical values. Photodissociation begins near 420 nm, ~20 nm above the nominal threshold at 398 nm. A second absorption region below 250 nm consists of a continuum overlapped by well-defined bands. In this region, photodissociation leads at least partly to the formation of O (¹D) (threshold 244 nm).

Table 6.13b Quantum yield for the process NO₂ + *hν* → NO + O (³P) at 298 and 248 K^a

λ (nm)	ϕ_{298}	ϕ_{248}	λ (nm)	ϕ_{298}	ϕ_{248}	λ (nm)	ϕ_{298}	ϕ_{248}	λ (nm)	ϕ_{298}	ϕ_{248}
300–398	1.00	1.00	403	0.53	0.44	408	0.22	0.14	413	0.09	0.06
399	0.95	0.94	404	0.44	0.34	409	0.18	0.12	414	0.08	0.04
400	0.88	0.86	405	0.37	0.28	410	0.15	0.10	415	0.06	0.03
401	0.75	0.69	406	0.30	0.22	411	0.13	0.08	416	0.05	0.02
402	0.62	0.56	407	0.26	0.18	412	0.11	0.07	417	0.04	0.02

^aFrom the critical assessment of data by Troe (2000)

Table 6.14a Absorption cross sections of nitrogen trioxide, NO₃ (298 K)^a

λ (nm)	$10^{19} \sigma$ (cm ²)	λ (nm)	$10^{19} \sigma$ (cm ²)	λ (nm)	$10^{19} \sigma$ (cm ²)	λ (nm)	$10^{19} \sigma$ (cm ²)	λ (nm)	$10^{19} \sigma$ (cm ²)
410	0.1	488	10.3	566	30.9	613	28.6	652	6.6
412	0.5	490	11.2	568	30.9	614	27.7	653	7.7
414	0.2	492	10.8	570	30.3	615	24.5	654	8.9
416	0.7	494	11.0	572	29.8	616	22.7	655	10.6
418	0.5	496	13.1	574	31.0	617	22.9	656	14.4
420	0.9	498	13.0	576	35.5	618	25.9	657	18.6
422	1.0	500	12.3	578	35.9	619	27.8	658	26.3
424	1.0	502	12.0	580	36.3	620	35.5	659	44.2
426	1.5	504	13.7	582	35.6	621	56.9	660	80.9
428	1.3	506	14.5	583	31.8	622	110.5	661	157.2
430	1.8	508	13.8	584	30.6	623	159.9	662	228.0
432	1.6	510	16.4	585	31.4	624	130.8	663	189.4
434	2.0	512	19.2	586	36.0	625	91.0	664	122.6
436	1.6	514	17.1	587	45.2	626	79.3	665	80.5
438	2.3	516	16.9	588	54.7	627	81.7	666	53.9
440	2.1	518	15.6	589	66.5	628	80.0	667	33.0
442	2.3	520	18.2	590	64.7	629	75.8	668	20.6
444	2.1	522	20.9	591	59.1	630	73.4	669	13.6
446	2.6	524	17.8	592	55.5	631	52.5	670	10.3
448	2.6	526	17.7	593	49.7	632	35.8	671	8.6
450	3.1	528	22.8	594	45.5	633	23.6	672	8.2
452	3.6	530	24.2	595	46.6	634	17.8	673	7.0
454	3.9	532	21.9	596	50.2	635	15.6	674	5.6
456	3.8	534	22.1	597	47.3	636	18.3	675	5.2
458	4.0	536	27.9	598	39.8	637	22.5	676	5.3
460	4.3	538	25.4	599	33.7	638	22.0	677	6.4
462	4.3	540	22.8	600	30.0	639	17.1	678	8.1
464	5.2	542	20.4	601	31.1	640	13.4	679	8.5
466	5.9	544	18.5	602	36.0	641	10.9	680	7.5
468	6.1	546	26.3	603	41.3	642	10.0	681	5.8
470	6.4	548	32.4	604	47.4	643	10.5	682	4.3
472	7.0	550	26.9	605	47.3	644	10.3	683	3.3
474	6.7	552	26.8	606	36.0	645	9.3	684	2.8
476	8.5	554	30.2	607	26.1	646	8.1	685	1.9
478	7.9	556	35.4	608	20.1	647	7.6	686	1.7
480	7.6	558	38.1	609	18.6	648	6.7	687	1.3
482	7.7	560	36.0	610	19.2	649	5.9	688	1.3
484	8.4	562	31.5	611	20.7	650	5.4	689	1.3
486	9.9	564	29.5	612	24.2	651	6.0	690	1.1

^aSource of data: Sander (1986), abbreviated

Comment: The band maxima increase significantly with decreasing temperature. The following formula was suggested by Orphal et al. (2003) to account for the effect:

$$\sigma(T) / \sigma(298\text{K}) = \left\{ 1 - \exp(-A/T) - 2 \exp(-B/T) \right\} / \left\{ 1 - \exp(-A/298) - 2 \exp(-B/298) \right\}$$

where $A = 1096.4$ and $B = 529.5$ are the vibrational energies divided by the Boltzmann constant.

Table 6.14b Quantum yields for the photodissociation of NO_3 at 298 and 230 K^a

λ (nm)	298 K		230 K		λ (nm)	298 K		230 K	
	ϕ_1	ϕ_2	ϕ_1	ϕ_2		ϕ_1	ϕ_2	ϕ_1	ϕ_2
585	0.983	0.0	0.996	0.0	615	0.147	0.166	0.058	0.110
590	0.793	0.190	0.696	0.300	620	0.090	0.131	0.030	0.072
595	0.608	0.359	0.453	0.359	625	0.049	0.099	0.014	0.045
600	0.472	0.291	0.307	0.346	630	0.026	0.065	0.006	0.025
605	0.323	0.264	0.176	0.253	635	0.015	0.037	0.003	0.012
610	0.226	0.236	0.105	0.193	640	0.007	0.020	0.001	0.005

^aFor the two processes: $\text{NO}_3 + h\nu \rightarrow \text{NO}_2(^2A_1) + \text{O}(^3P)$ (ϕ_1) and $\text{NO}_3 + h\nu \rightarrow \text{NO}(^2\Pi) + \text{O}_2(X^3\Sigma_g^-)$ (ϕ_2). Source of data: Johnston et al. (1996), abbreviated

Table 6.15 Absorption cross sections of N_2O (298 K)^a

λ (nm)	$10^{20} \sigma$		$10^{20} \sigma$		$10^{20} \sigma$		$10^{21} \sigma$		$10^{22} \sigma$	
	(cm^2)	λ (nm)	(cm^2)	λ (nm)	(cm^2)	λ (nm)	(cm^2)	λ (nm)	(cm^2)	
165	5.61	182	14.7	193	8.95	204	23.0	220	9.22	
170	8.30	183	14.6	194	8.11	205	19.5	222	5.88	
173	11.3	184	14.4	195	7.57	206	16.5	224	3.75	
174	11.9	185	14.3	196	6.82	207	13.8	226	2.39	
175	12.6	186	13.6	197	6.10	208	11.6	228	1.51	
176	13.4	187	13.1	198	5.35	209	9.80	230	0.955	
177	14.0	188	12.5	199	4.70	210	7.55	232	0.605	
178	13.9	189	11.7	200	4.09	212	5.18	234	0.360	
179	14.4	190	11.1	201	3.58	214	3.42	236	0.240	
180	14.6	191	10.4	202	3.09	216	2.23	238	0.152	
181	14.6	192	9.75	203	2.67	218	1.42	240	0.101	

^aSource of data: Hubrich and Stuhl (1980), Selwyn et al. (1977). Temperature dependence (for the range: 173–240 nm, 194–302 K): $\ln \sigma(\lambda, T) = \sum A_n \lambda^n + (T-300) \exp(\sum B_m \lambda^m)$, $n=0-4$: $A_0=68.21023$, $A_1=-4.071805$, $A_2=4.301146 \times 10^{-2}$, $A_3=-1.777846 \times 10^{-4}$, $A_4=2.520672 \times 10^{-7}$; $m=0-3$: $B_0=123.4014$, $B_1=-2.116255$, $B_2=1.111572 \times 10^{-2}$, $B_3=-1.881058 \times 10^{-5}$. The photodissociation process is: $\text{N}_2\text{O} + h\nu \rightarrow \text{N}_2 + \text{O}(^1D)$, $\phi = 1.0$

Table 6.16 Absorption cross sections of N_2O_5 (298 K)^a

λ (nm)	$10^{19} \sigma$ (cm^2)	λ (nm)	$10^{20} \sigma$ (cm^2)	λ (nm)	$10^{21} \sigma$ (cm^2)	λ (nm)	$10^{21} \sigma$ (cm^2)	λ (nm)	$10^{22} \sigma$ (cm^2)
170	332	290	6.52	322	10.50	348	2.34	374	5.45
180	225	295	5.02	324	9.30	350	2.10	376	4.84
190	149	300	3.81	326	8.26	352	1.88	378	4.31
200	90.0	302	3.40	328	7.35	354	1.67	380	3.83
210	38.0	304	3.03	330	6.54	356	1.49	382	3.41
220	16.5	306	2.70	332	5.82	358	1.33	384	3.05
230	8.38	308	2.40	334	5.18	360	1.20	386	2.73
240	5.71	310	2.13	336	4.62	362	1.07	388	2.42
250	3.86	312	1.90	338	4.12	364	0.958	390	2.15
260	2.52	314	1.68	340	3.68	366	0.852	392	1.93
270	1.62	316	1.49	342	3.28	368	0.763	394	1.72
280	1.05	318	1.33	344	2.93	370	0.685	396	1.50
285	8.34	320	1.18	346	2.62	372	0.613	398	1.34

^aSource of data: Harwood et al. (1998), 210–398 nm, Osborne et al. (2000), 170–200 nm

Comments: The maximum of absorption occurs at $\lambda \sim 160$ nm. In the wavelength region covered the absorption cross section is a smoothly varying function of λ . At wavelengths < 280 nm the temperature dependence is insignificant. Yao et al. (1982) have provided a simple formula for the temperature effect:

$$\ln(10^{19} \sigma) = 0.432537 + (4728.48 - 17.1269\lambda) / T$$

covering the wavelength region 280–380 nm and the temperature interval 225–300 K. Harwood et al. (1993) have presented a different algorithm for calculating the temperature dependence, although their data are in good agreement with those of Yao et al. (1982).

Quantum yield: $N_2O_5 + h\nu \rightarrow NO_3 + NO_2$ (ϕ_1), $N_2O_5 + h\nu \rightarrow NO_3 + NO + O$ (ϕ_2), $\lambda > 300$ nm: $\phi_1 \approx 1$, $\lambda < 300$ nm: ϕ_1 decreases toward ϕ_1 0.7–0.8 at 248 nm while ϕ_2 increases from $\phi_2 = 0.15$ at 289 nm toward 0.72 at 248 nm.

Table 6.17 Absorption cross sections of nitrous acid, HNO₂ (298 K)^a

λ (nm)	$10^{20} \sigma$ (cm ²)	λ (nm)	$10^{20} \sigma$ (cm ²)	λ (nm)	$10^{20} \sigma$ (cm ²)	λ (nm)	$10^{21} \sigma$ (cm ²)	λ (nm)	$10^{22} \sigma$ (cm ²)
296	0.326	321	5.96	339.5	9.96	355	27.64	372	7.96
297	0.565	322	4.05	340	7.79	355.5	16.40	373	6.30
298	0.517	323	4.56	340.5	8.51	356	11.13	374	4.57
299	0.429	324	5.89	341	16.13	357	9.45	375	3.55
300	0.617	325	4.05	341.5	31.52	357.5	10.08	376	3.36
301	0.690	326	2.65	342	29.40	358	9.84	377	3.66
302	0.579	326.5	3.55	342.5	18.47	359	8.37	378	4.33
303	0.925	327	6.44	343	11.43	360	6.87	379	5.66
304	1.04	327.5	10.26	343.5	8.29	361	6.05	380	7.21
305	1.57	328	9.22	344	7.59	362	5.98	381	9.13
306	1.29	328.5	6.38	345	8.77	363	7.39	382	12.44
307	0.916	329	5.20	346	9.64	364	11.49	383	17.03
308	1.45	330	9.92	347	7.80	364.5	12.71	384	19.47
309	2.01	330.5	15.06	348	6.63	365	12.82	385	16.09
310	1.51	331	14.32	349	6.00	365.5	13.19	386	10.52
311	2.07	331.5	9.88	350	9.06	366	14.84	387	6.59
312	2.42	332	6.94	350.5	14.95	366.5	18.43	388	4.30
313	2.25	333	6.31	351	16.94	367	25.08	389	2.81
314	3.35	334	8.35	351.5	14.07	367.5	35.18	390	1.71
315	2.54	335	7.71	352	12.42	368	43.56	391	0.992
316	1.61	336	5.33	352.5	12.81	368.5	41.37	392	0.731
317	3.21	337	4.23	353	16.34	369	31.45	393	0.597
318	4.49	338	9.38	353.5	28.49	369.5	21.72	394	0.528
319	3.19	338.5	16.52	354	48.73	370	15.05	395	0.403
320	4.66	339	14.32	354.5	44.34	371	9.49	396	0.237

^aSource of data: Stutz et al. (2000). The photodissociation process HNO₂ + $h\nu$ → NO + OH occurs with quantum yield $\phi \approx 1.0$

Table 6.18 Absorption cross sections of H₂O₂, HO₂NO₂ and HNO₃^a

λ (nm)	H ₂ O ₂	HO ₂ NO ₂	HNO ₃		λ (nm)	H ₂ O ₂	HO ₂ NO ₂	HNO ₃	
	$10^{20} \sigma$ (cm ²)	$10^{20} \sigma$ (cm ²)	$10^{20} \sigma$ (cm ²)	$10^3 B$ (K ⁻¹)		$10^{20} \sigma$ (cm ²)	$10^{20} \sigma$ (cm ²)	$10^{20} \sigma$ (cm ²)	$10^3 B$ (K ⁻¹)
190	67.2	1,010	1,360	0	235	15.0	68.0	3.75	1.93
195	56.3	816	1,016	0	240	12.4	57.9	2.58	1.97
200	47.5	563	588	1.66	245	10.2	49.7	2.11	1.68
205	40.8	367	288	1.75	250	8.3	41.1	1.97	1.34
210	35.7	239	104	1.97	255	6.7	34.9	1.95	1.16
215	30.7	161	36.5	2.17	260	5.3	28.4	1.91	1.14
220	25.8	118	14.9	2.15	265	4.2	22.9	1.80	1.20
225	21.7	93.2	8.81	1.90	270	3.3	18.0	1.62	1.45
230	18.2	78.8	5.78	1.80	275	2.6	13.3	1.38	1.60

(continued)

Table 6.18 (continued)

λ (nm)	H_2O_2	HO_2NO_2	HNO_3		λ (nm)	H_2O_2	HO_2NO_2	HNO_3	
	$10^{20} \sigma$ (cm^2)	$10^{20} \sigma$ (cm^2)	$10^{20} \sigma$ (cm^2)	10^3 B (K^{-1})		$10^{20} \sigma$ (cm^2)	$10^{20} \sigma$ (cm^2)	$10^{20} \sigma$ (cm^2)	10^3 B (K^{-1})
280	2.0	9.3	1.12	1.78	320	0.22	0.24	0.020	6.45
285	1.5	6.2	0.858	1.99	325	0.16	0.15	0.0095	7.35
290	1.2	3.9	0.615	2.27	330	0.13	0.09	0.0043	9.75
295	0.90	2.4	0.412	2.61	335	0.10	–	0.0022	10.1
300	0.68	1.4	0.263	3.10	340	0.07	–	0.0010	11.8
305	0.51	0.85	0.150	3.64	345	0.05	–	0.0006	11.2
310	0.39	0.53	0.081	4.23	350	0.04	–	0.0004	9.30
315	0.29	0.39	0.041	5.20					

^aAbsorption cross sections at 298 K; the temperature dependence for HNO_3 is expressed by $\sigma(\lambda, T) = \sigma(\lambda, 298) \exp(B(\lambda)(T-298))$, with $B(\lambda)$ shown next to the cross sections. Source of data: Sander et al. (2006) (review)

Quantum yields (for the predominant photodissociation processes)

- (a) $\text{H}_2\text{O}_2 + h\nu \rightarrow 2 \text{ OH}$ (ϕ_1), $\text{H}_2\text{O}_2 + h\nu \rightarrow \text{H} + \text{HO}_2$ (ϕ_2), $\lambda > 230 \text{ nm}$: $\phi_1 \approx 1$, $\phi_2 = 0$; $\lambda = 193 \text{ nm}$: $\phi_2 = 0.15$ ($\phi_1 = 0.85$ by difference).
- (b) $\text{HO}_2\text{NO}_2 + h\nu \rightarrow \text{HO}_2 + \text{NO}_2$ (ϕ_1), $\text{HO}_2\text{NO}_2 + h\nu \rightarrow \text{OH} + \text{NO}_3$ (ϕ_2), $\lambda > 248 \text{ nm}$: $\phi_1 \approx 0.9$, $\phi_2 = 0.08$; $\lambda = 193 \text{ nm}$: $\phi_1 \approx 0.56$, $\phi_2 = 0.35$ (Jimenez et al. 2005);
- (c) $\text{HNO}_3 + h\nu \rightarrow \text{OH} + \text{NO}_2$ (ϕ_1), $\text{HNO}_3 + h\nu \rightarrow \text{O} + \text{NO}_3$ (ϕ_2), $\lambda = 248 \text{ nm}$: $\phi_1 = 0.95$, $\phi_2 = 0.03$; $\lambda = 222 \text{ nm}$: $\phi_1 = 0.90$; $\lambda = 193 \text{ nm}$: $\phi_1 = 0.33$, $\phi_2 = 0.67$ (Sander et al. 2006).

Table 6.19a Absorption cross sections of formaldehyde^a

λ (nm)	$10^{20} \sigma$ (cm^2)	λ (nm)	$10^{20} \sigma$ (cm^2)	λ (nm)	$10^{20} \sigma$ (cm^2)	λ (nm)	$10^{20} \sigma$ (cm^2)
240	0.078	255	0.450	270	0.963	285	4.050
241	0.078	256	0.628	271	1.941	286	2.095
242	0.123	257	0.443	272	1.430	287	1.153
243	0.159	258	0.307	273	0.811	288	3.169
244	0.110	259	0.617	274	0.658	289	3.225
245	0.131	260	0.605	275	2.143	290	1.173
246	0.163	261	0.659	276	2–584	291	1.836
247	0.151	262	0.603	277	1.573	292	0.797
248	0.234	263	1.077	278	1.035	293	3.128
249	0.318	264	0.947	279	2.451	294	7.154
250	0.257	265	0.531	280	23.38	295	4.054
251	0.204	266	0.539	281	1.562	296	2.474
252	0.337	267	1.360	282	0.973	297	1.467
253	0.289	268	1.243	283	0.722	298	4.217
254	0.342	269	0.991	284	4.265	299	3.175

(continued)

Table 6.19a (continued)

λ (nm)	$10^{20} \sigma$ (cm ²)	λ (nm)	$10^{20} \sigma$ (cm ²)	λ (nm)	$10^{20} \sigma$ (cm ²)	λ (nm)	$10^{20} \sigma$ (cm ²)
300	0.964	319	0.978	338	1.919	357	0.0345
301	1.625	320	1.194	339	5.381	358	0.0186
302	0.854	321	1.598	340	3.151	359	0.0111
303	3.021	322	0.722	341	0.978	360	0.0087
304	7.219	323	0.328	342	0.509	361	0.0100
305	4.752	324	0.858	343	1.922	362	0.0211
306	4.292	325	1.578	344	1.268	363	0.0141
307	1.781	326	6.876	345	0.437	364	0.0094
308	1.385	327	4.370	346	0.119	365	0.0088
309	3.252	328	1.220	347	0.044	366	0.0085
310	1.737	329	3.120	348	0.075	367	0.0091
311	0.462	330	3.865	349	0.038	368	0.0142
312	1.188	331	1.412	350	0.036	369	0.0297
313	0.964	332	0.347	351	0.089	370	0.0635
314	5.637	333	0.214	352	0.729	371	0.0571
315	5.565	334	0.159	353	2.275	372	0.0198
316	2.561	335	0.097	354	1.645	373	0.0113
317	5.777	336	0.126	355	0.696	374	0.0091
318	3.151	337	0.383	356	0.148	375	0.0087

^aTemperature 298 K; Source of data Meller and Moortgat (2000)

Product channels are: $\text{HCHO} + h\nu \rightarrow \text{H} + \text{CHO}$ (ϕ_1), $\text{HCHO} + h\nu \rightarrow \text{H}_2 + \text{CO}$ (ϕ_2). Quantum yields vary with wavelength. They are independent of temperature and pressure at wavelengths $\lambda < 330$ nm, but show Stern-Volmer pressure dependence at $\lambda > 330$ nm.

Table 6.19b Quantum yields of HCHO in air at 1 atm (101,325 Pa) and 298 K^a

λ	ϕ_1	ϕ_2	λ	ϕ_1	ϕ_2	λ	ϕ_1	ϕ_2	λ	ϕ_1	ϕ_2
250	0.31	0.49	280	0.56	0.34	310	0.75	0.25	340	0	0.66
255	0.30	0.50	285	0.64	0.30	315	0.72	0.28	345	0	0.51
260	0.31	0.49	290	0.68	0.29	320	0.61	0.40	350	0	0.38
265	0.32	0.48	295	0.75	0.26	325	0.46	0.64	355	0	0.23
270	0.38	0.45	300	0.77	0.23	330	0.30	0.67	360	0	0.07
275	0.45	0.39	305	0.78	0.22	335	0.14	0.68	365	0	~ 0

^aWavelength λ (nm); quantum yields derived by interpolation of data reported by Moortgat et al. (1983) and earlier studies cited therein

The observed pressure dependence is $(\phi_2(\lambda, n, T))^{-1} = (\phi_{\text{CO}}(\lambda, n, T))^{-1} = 1 + \alpha(\lambda, T) n$, where n (molecule cm⁻³) is the number density of air; $\alpha(\lambda, T)$ (10⁻¹⁹ cm³ molecule⁻¹) is the quenching coefficient:

$$\begin{array}{ccc} & \alpha(298\text{K}) & \alpha(220\text{K}) \\ \lambda = 339[\text{nm}] & 0.26 \pm 0.10 & 0.39 \pm 0.07 \\ \lambda = 353[\text{nm}] & 1.12 \pm 0.17 & 2.47 \pm 0.59 \end{array}$$

Table 6.20 Absorption cross sections of acetaldehyde, CH₃CHO at 298 K^a

λ (nm)	$10^{20} \sigma$		$10^{20} \sigma$		$10^{20} \sigma$		$10^{20} \sigma$		$10^{20} \sigma$	
	(cm ²)	λ (nm)	(cm ²)	λ (nm)	(cm ²)	λ (nm)	(cm ²)	λ (nm)	(cm ²)	
210	0.049	295	4.27	309	3.14	323	1.24	337	0.222	
220	0.059	296	4.24	310	2.93	324	1.09	338	0.205	
230	0.151	297	4.38	311	2.76	325	1.14	339	0.219	
240	0.469	298	4.41	312	2.53	326	1.07	340	0.150	
250	1.13	299	4.26	313	2.47	327	0.858	341	0.074	
260	2.22	300	4.16	314	2.44	328	0.747	342	0.042	
270	3.42	301	3.99	315	2.20	329	0.707	343	0.031	
280	4.50	302	3.86	316	2.04	330	0.688	344	0.026	
285	4.49	303	3.72	317	2.07	331	0.588	345	0.021	
290	4.89	304	3.48	318	1.98	332	0.530	346	0.019	
291	4.78	305	3.42	319	1.87	333	0.398	347	0.015	
292	4.68	306	3.42	320	1.72	334	0.363	348	0.016	
293	4.53	307	3.36	321	1.48	335	0.350	349	0.010	
294	4.33	308	3.33	322	1.40	336	0.238	350	0.008	

^aSource of data: Martinez et al. (1992)

Quantum yields: The main processes are (1) CH₃CHO + $h\nu$ → CH₃ + CHO (ϕ_1), which is active in the entire wavelength region, and (2) CH₃CHO + $h\nu$ → CH₄ + CO (ϕ_2), which occurs at wavelengths below $\lambda \approx 290$ nm so that it is inactive in the troposphere.

Table 6.20a Acetaldehyde quantum yields in air at 1 atm (101,325 Pa) and 295 K^a

λ (nm)	290	295	300	305	310	315	320	325	330
$\phi_{1\text{atm}}$	0.63	0.57	0.50	0.42	0.32	0.20	0.09	0.04	0.01

^aSource of data: Moortgat et al. (2010); quantum yields increase with decreasing pressure in accordance with the Stern-Volmer relation and may be estimated for any reduced pressure p (atm) from $\phi_1 = (1 + kp)^{-1}$ with k (atm⁻¹) = $(1 - \phi_{1\text{atm}})/\phi_{1\text{atm}}$

Table 6.21 Absorption cross sections of acetone, CH₃COCH₃, at 295 and 230 K^a

λ (nm)	$10^{20} \sigma$ (cm ²)		$10^{20} \sigma$ (cm ²)		$10^{20} \sigma$ (cm ²)		$10^{21} \sigma$ (cm ²)	
	295 K	230 K	λ (nm)	295 K	230 K	λ (nm)	295 K	230 K
215	0.167	0.169	255	3.15	3.17	291	3.95	3.64
220	0.246	0.250	260	3.81	3.81	292	3.82	3.50
225	0.380	0.390	265	4.41	4.37	293	3.71	3.39
230	0.584	0.599	270	4.79	4.71	294	3.57	3.25
235	0.885	0.906	275	4.94	4.78	295	3.42	3.10
240	1.30	1.33	280	4.91	4.706	296	3.26	2.93
245	1.83	1.86	285	4.54	4.26	297	3.11	2.76
250	2.47	2.50	290	4.06	3.75	298	2.98	2.65

(continued)

Table 6.21 (continued)

λ (nm)	$10^{20} \sigma$ (cm ²)		λ (nm)	$10^{20} \sigma$ (cm ²)		λ (nm)	$10^{20} \sigma$ (cm ²)		λ (nm)	$10^{21} \sigma$ (cm ²)	
	295 K	230 K		295 K	230 K		295 K	230 K		295 K	230 K
307	1.75	1.48	318	0.598	0.451	329	0.0913	0.0423	340	0.0912	0.0516
308	1.61	1.35	319	0.523	0.385	330	0.0740	0.0331	341	0.0729	0.0418
309	1.49	1.23	320	0.455	0.324	331	0.0586	0.0258	342	0.0583	0.0331
310	1.36	1.17	321	0.411	0.280	332	0.465	0.204	343	0.0494	0.0275
311	1.24	1.00	322	0.348	0.227	333	0.375	0.165	344	0.0365	0.0194
312	1.14	0.916	323	0.294	0.183	334	0.311	0.139	345	0.0301	0.0156
313	1.06	0.846	324	0.248	0.147	335	0.248	0.114	346	0.0235	0.0124
314	0.944	0.749	325	0.210	0.118	336	0.199	0.0953	347	0.0158	0.0089
315	0.837	0.658	326	0.174	0.0929	337	0.162	0.0812	348	0.0111	0.0069
316	0.760	0.591	327	0.141	0.0718	338	0.135	0.0709	349	0.0107	0.0069
317	0.684	0.525	328	0.113	0.0549	339	0.113	0.0618			

^aSource of data: Gierczak et al. (1998)

Quantum yields: The main processes are (1) $\text{CH}_3\text{COCH}_3 + h\nu \rightarrow \text{CH}_3 + \text{CH}_3\text{CO}$ (ϕ_1) and (2) $\text{CH}_3\text{COCH}_3 + h\nu \rightarrow 2\text{CH}_3 + \text{CO}$ (ϕ_2); under tropospheric conditions, i.e. $\lambda > 290$ nm, $\phi_2 = \phi_{\text{CO}} \leq 0.05$, so that it may be neglected to a first approximation. Warneck (2001) has derived an expression for the dependence of ϕ_1 on wavelength (nm) and air number density n_M (molecule cm⁻³): $\phi_1 = \{(1/\Phi_S) + 7.145 \times 10^{-7} n_M \exp(-8780.6/\lambda)\}^{-1}$, where $\Phi_S = 0.113 + 0.887 [1 + \exp(\lambda - 307.5)/3.0]^{-1}$, ($T \approx 295$ K). Blitz et al. (2004), who have studied the temperature dependence of the quantum yield, prefer different formulae.

Table 6.22 Absorption cross sections of methyl iodide^a

λ (nm)	$10^{20} \sigma$		10^3 B	ϕ_2	λ (nm)	$10^{20} \sigma$		10^3 B	ϕ_2	λ (nm)	$10^{21} \sigma$		10^3 B	ϕ_2
	(cm ²)	(K ⁻¹)				(cm ²)	(K ⁻¹)				(cm ²)	(K ⁻¹)		
235	18.66	0.67	0.69	280	26.28	2.43	0.69	325	1.12	6.79	0.47			
240	35.18	0.61	0.71	285	14.18	3.74	0.62	330	0.64	7.82	0.72			
245	60.56	0.34	0.73	290	7.351	4.98	0.57	335	0.36	9.34	0.94			
250	88.46	0.08	0.75	295	3.736	6.38	0.52	340	0.21	10.95				
255	106.4	0.08	0.76	300	1.946	6.97	0.47	345	0.11	13.58				
260	107.2	-0.10	0.78	305	1.029	6.84	0.43	350	0.059	16.83				
265	92.03	-0.12	0.79	310	0.579	6.78	0.41	355	0.032	18.91				
270	68.14	0.54	0.76	315	0.334	6.75	0.40	360	0.019	17.28				
275	44.76	1.33	0.72	320	0.192	6.53	0.41	365	0.009	23.63				

^aAbsorption cross sections at 298 K; the temperature dependence is expressed by $\ln \sigma(\lambda, T) = \ln \sigma(\lambda, 298) + B(\lambda)(T - 298)$, with $B(\lambda)$ shown next to the cross sections. Source of data: Rattigan et al. (1997). ϕ_2 is the quantum yield for the formation of I (²P_{1/2}) atoms

Quantum yields: Photodissociation produces iodine atoms in the ²P_{3/2} ground state as well as in the metastable ²P_{1/2} state, which lies ~0.943 eV above the ground state: $\text{CH}_3\text{I} + h\nu \rightarrow \text{CH}_3 + \text{I}(\text{P}_{3/2})$ (ϕ_1), $\text{CH}_3\text{I} + h\nu \rightarrow \text{CH}_3 + \text{I}(\text{P}_{1/2})$ (ϕ_2). The total quantum

yield is unity ($\phi_1 + \phi_2 = 1$). Values of ϕ_2 listed in Table 6.22 were derived by interpolation of quantum yields measured in the wavelength range 222–333.5 nm by Kang et al. (1996), Ogorzalek et al. (1989) and Uma and Das (1994). The strong increase of ϕ_2 at wavelengths approaching the onset of absorption suggests that in this wavelength region $\phi_2 \approx 1$.

Table 6.23 Absorption cross sections of carbonyl sulfide, OCS, at 295 and 225 K^a

λ (nm)	$10^{20} \sigma$ (cm ²)		λ (nm)	$10^{20} \sigma$ (cm ²)		λ (nm)	$10^{21} \sigma$ (cm ²)		λ (nm)	$10^{22} \sigma$ (cm ²)	
	295 K	225 K		295 K	225 K		295 K	225 K		295 K	225 K
185	27.8	21.2	214	22.2	22.2	246	31.8	20.5	276	1.25	0.561
186	18.8	12.5	215	23.9	23.1	248	22.8	14.0	277	1.01	0.396
187	10.5	7.02	216	26.1	25.3	250	16.1	9.74	278	0.721	0.281
188	7.73	5.09	218	28.3	26.9	252	11.1	6.13	279	0.831	0.250
189	4.39	2.76	220	31.9	30.2	254	7.72	4.06	280	0.615	0.238
190	3.41	2.35	222	31.5	29.4	255	6.42	3.32	281	0.429	0.144
191	2.37	1.62	224	31.7	28.9	256	5.38	2.71	282	0.318	0.116
192	1.97	1.58	225	31.2	28.4	258	3.65	1.71	283	0.315	0.131
194	1.81	1.64	226	30.6	27.9	260	2.41	1.11	284	0.298	0.099
195	1.92	1.81	228	27.8	24.6	262	1.62	0.730	285	0.181	0.061
196	2.16	2.10	230	24.6	21.5	264	1.13	0.493	286	0.141	0.062
198	2.85	2.82	232	21.0	17.6	265	0.12	0.403	287	0.154	0.068
200	3.84	3.83	234	16.9	13.8	266	0.77	0.339	288	0.128	0.048
202	5.13	5.15	235	15.1	12.0	268	0.52	0.214	289	0.076	0.034
204	7.02	7.06	236	13.6	10.7	270	0.369	0.152	290	0.057	0.031
205	7.96	8.02	238	10.5	7.96	271	0.297	0.116	291	0.062	0.036
206	9.39	9.48	240	8.00	5.78	272	0.250	0.106	292	0.061	0.024
208	12.0	12.1	242	6.02	4.20	273	0.222	0.0921	293	0.032	0.015
210	15.0	15.1	244	4.35	2.88	274	0.168	0.0630	294	0.019	0.011
212	18.1	18.1	245	3.76	2.46	275	0.136	0.0526	295	0.029	0.015

^aSource of data: Molina et al. (1981). Carbonyl sulfide features a broad absorption continuum with superimposed band structure at wavelengths $\lambda > 275$ nm and at the absorption maximum near 225 nm

Quantum yields: Photodissociation processes are (1) $\text{OCS} + h\nu \rightarrow \text{CO} + \text{S} (^3\text{P})$ (ϕ_1) and (2) $\text{OCS} + h\nu \rightarrow \text{CO} + \text{S} (^1\text{D})$ (ϕ_2). The second process is dominant; $\phi_1 + \phi_2 = 1.0$ (Zhao et al. 1995), $\phi_1 \approx 0.05$ at 220 nm (Nan et al. 1993).

Table 6.24 Absorption cross sections of carbon tetrachloride, CCl_4 , at 295 and 210 K^a

λ (nm)	$10^{18} \sigma$ (cm ²)		λ (nm)	$10^{18} \sigma$ (cm ²)		λ (nm)	$10^{18} \sigma$ (cm ²)		λ (nm)	$10^{18} \sigma$ (cm ²)	
	295 K	210 K		295 K	210 K		295 K	210 K		295 K	210 K
174	9.90	9.90	180	7.20	7.20	186	3.10	3.10	192	0.992	0.992
176	10.10	10.10	182	5.90	5.90	188	1.98	1.98	194	0.767	0.767
178	9.75	9.75	184	4.40	4.40	190	1.469	1.469	196	0.695	0.695

(continued)

Table 6.24 (continued)

λ (nm)	$10^{19} \sigma$ (cm ²)		$10^{19} \sigma$ (cm ²)			$10^{20} \sigma$ (cm ²)			$10^{20} \sigma$ (cm ²)		
	295 K	210 K	λ (nm)	295 K	210 K	λ (nm)	295 K	210 K	λ (nm)	295 K	210 K
198	6.80	6.80	212	4.10	3.48	226	7.60	4.45	240	0.83	0.342
200	6.60	6.60	214	3.45	2.79	228	5.65	3.16	242	0.59	0.234
202	6.38	6.38	216	2.78	2.17	230	4.28	2.27	244	0.413	0.258
204	6.10	6.01	218	2.21	1.63	232	3.04	1.52	246	0.29	0.108
206	5.70	5.44	220	1.75	1.25	234	2.20	1.05	248	0.21	0.0762
208	5.25	4.83	222	1.36	0.900	236	1.60	0.723	250	0.148	0.0528
210	4.69	4.15	224	1.02	0.640	238	1.16	0.50			

^aData source: Simon et al. (1988)

Comments: Simon et al. (1988) have approximated wavelength and temperature dependence of the cross section by means of the expression $\log_{10} \sigma(\lambda, T) = \Sigma A_n \lambda^n + (T-273) \Sigma B_n \lambda^n$ ($n=0-4$), covering the wavelength region 194–250 nm and the temperature range 210–300 K, with the following parameters

$$A_0 = -37.104, A_1 = -5.8218 \times 10^{-1}, A_2 = 9.9974 \times 10^{-3}, A_3 = -4.6765 \times 10^{-5}, \\ A_4 = 6.8501 \times 10^{-8}; B_0 = 1.0739, B_1 = -1.6275 \times 10^{-2}, B_2 = 8.8141 \times 10^{-5}, B_3 = -1.9811 \times 10^{-7}, \\ B_4 = 1.5022 \times 10^{-10}.$$

Quantum yields: The principal photolytic processes are (1) $\text{CCl}_4 + h\nu \rightarrow \text{CCl}_3 + \text{Cl}$ (ϕ_1) and (2) $\text{CCl}_4 + h\nu \rightarrow \text{CCl}_2 + 2 \text{Cl}$ (ϕ_2), with $\phi_1 + \phi_2 \approx 1.0$. At the long-wavelength limit $\phi_2 \approx 0$, but ϕ_2 increases at the expense of ϕ_1 until near 165 nm both processes occur with essentially equal probability (Rebbert and Ausloos 1977).

Quantum yields for CFCl_3 and CF_2Cl_2 behave similarly (Rebbert and Ausloos 1975) (absorption cross sections for these two compounds are given in the next table).

Table 6.25 Absorption cross sections of CFCl_3 and CF_2Cl_2 at 295 and 210 K^a

λ (nm)	$10^{19} \sigma$ (cm ² molecule ⁻¹)				λ (nm)	$10^{20} \sigma$ (cm ² molecule ⁻¹)			
	CFCl_3		CF_2Cl_2			CFCl_3		CF_2Cl_2	
	295 K	210 K	295 K	210 K		295 K	210 K	295 K	210 K
174	31.30	31.30	16.20	16.20	204	37.4	30.0	0.344	0.169
176	32.40	32.40	18.10	18.10	206	28.0	21.6	0.209	0.989
178	32.35	32.35	18.70	18.70	208	19.7	14.9	0.127	0.557
180	31.40	31.40	17.90	17.90	210	14.8	9.94	0.759	0.324
182	29.60	29.60	16.00	16.00	212	10.5	6.63	0.454	0.183
184	27.20	27.20	13.40	13.40	214	7.56	4.31	0.271	0.106
186	24.30	23.00	10.70	10.70	216	5.38	2.78	0.158	0.0577
188	21.30	20.20	8.28	7.93	218	3.79	1.77	0.100	0.0330
190	17.90	17.05	6.32	5.29	220	2.64	1.13	0.060	0.0180
192	15.40	14.12	4.55	3.58	222	1.82	0.714	0.036	0.0105
194	12.43	11.51	3.15	2.28	224	1.24	0.454	0.022	0.0060
196	9.91	9.05	2.11	1.44	226	0.842	0.291	0.013	0.0034
198	7.80	7.18	1.39	0.882	228	0.565	0.188		
200	6.45	5.58	0.889	0.511	230	0.375	0.123		
202	5.00	4.20	0.551	0.297					

^aSource of data: Simon et al. (1988). For quantum yields see preceding entry

Comments: Mérienne et al. (1990) have studied the spectra of CFCl_3 and CF_2Cl_2 in the wavelength region 200–238 nm and 200–231 nm, respectively, and found good agreement with the data of Simon et al. (1988) except at long wavelengths where deviations up to 15% occurred. Simon et al. (1988) have used a formula for wavelength and temperature dependence of the cross sections similar to that for carbon tetrachloride, but the published parameters contain numerical errors. Mérienne et al. (1990) have used the expression $\ln \sigma(\lambda, T) = \sum A_n (200 - \lambda)^n + (T - 296) \times \sum B_n (200 - \lambda)^n$ ($n=0-3$, $220 < T$ (K) < 296), which represents their data quite accurately. CFCl_3 : $A_0 = -41.925548$, $A_1 = -1.142857 \times 10^{-1}$, $A_2 = -3.12034 \times 10^{-3}$, $A_3 = 3.6699 \times 10^{-5}$; $B_0 = 3.58977 \times 10^{-4}$, $B_1 = 3.02973 \times 10^{-4}$, $B_2 = -1.13 \times 10^{-8}$, $B_3 = 0$; CF_2Cl_2 : $A_0 = -43.8954569$, $A_1 = -2.403597 \times 10^{-1}$, $A_2 = -4.2619 \times 10^{-4}$, $A_3 = 9.8743 \times 10^{-6}$; $B_0 = 4.8438 \times 10^{-3}$, $B_1 = 4.96145 \times 10^{-4}$, $B_2 = -5.6953 \times 10^{-6}$, $B_3 = 0$.

Table 6.26a Absorption cross sections of chlorine nitrate, ClONO_2 , at 296 and 220 K^a

λ (nm)	$10^{18} \sigma$ (cm ²)		λ (nm)	$10^{19} \sigma$ (cm ²)		λ (nm)	$10^{21} \sigma$ (cm ²)		λ (nm)	$10^{21} \sigma$ (cm ²)	
	296 K	220 K		296 K	220 K		296 K	220 K		296 K	220 K
200	2.82	2.70	260	3.38	2.91	320	8.31	5.78	380	1.210	1.044
205	2.84	2.78	265	2.65	2.26	325	6.13	4.26	385	1.060	0.907
210	3.14	3.15	270	2.05	1.73	330	4.66	3.29	390	0.909	0.773
215	3.42	3.47	275	1.58	1.32	335	3.61	2.67	395	0.760	0.633
220	3.32	3.35	280	1.19	0.983	340	3.02	2.30	400	0.638	0.519
225	2.77	2.74	285	0.881	0.718	345	2.58	2.04	405	0.541	0.430
230	2.08	2.00	290	0.641	0.515	350	2.29	1.86	410	0.444	0.341
235	1.98	1.86	295	0.438	0.345	355	2.08	1.73	415	0.345	0.270
240	1.05	0.967	300	0.313	0.240	360	2.00	1.69	420	0.316	0.226
245	0.764	0.691	305	0.224	0.167	365	1.80	1.53	425	0.232	0.164
250	0.560	0.497	310	0.160	0.116	370	1.59	1.36	430	0.189	0.131
255	0.432	0.377	315	0.115	0.081	375	1.41	1.21			

^aSource of data : Burkholder et al. (1994); the authors presented wavelength-dependent parameters for the calculation of absorption coefficients from a second order polynomial in the temperature range 220–396 K

Quantum yields: The major processes at wavelengths above 220 nm are:

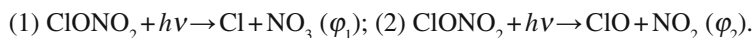


Table 6.26b Quantum yields for the photolysis of ClONO_2 ^a

λ	ϕ_1	ϕ_2	λ	ϕ_1	ϕ_2	λ	ϕ_1	ϕ_2	λ	ϕ_1	ϕ_2
240	0.48	0.52	270	0.57	0.43	300	0.68	0.32	330	0.80	0.20
250	0.50	0.50	280	0.61	0.39	310	0.72	0.28	340	0.85	0.15
260	0.54	0.46	290	0.64	0.36	320	0.76	0.24	350	0.90	0.10

^aWavelength λ (nm); quantum yields derived by interpolation of data summarized by Sander et al. (2006). At 193 and 220 nm the production of oxygen atoms is observed possibly indicating the occurrence of a third photolytic process

Table 6.27 Absorption cross sections of the chlorine oxide dimer, ClOOC1, at ~210 K^a

λ (nm)	$10^{20} \sigma$ (cm ²)	λ (nm)	$10^{20} \sigma$ (cm ²)	λ (nm)	$10^{20} \sigma$ (cm ²)	λ (nm)	$10^{20} \sigma$ (cm ²)	λ (nm)	$10^{20} \sigma$ (cm ²)
190	565	235	510	280	175	325	20	370	3.2
195	470	240	636	285	142	330	16	380	2.1
200	379	245	680	290	114	335	13	390	1.3
205	297	250	637	295	91	340	12	400	0.85
210	229	255	531	300	71	345	9.5	410	0.54
215	188	260	414	305	55	350	7.7	420	0.35
220	188	265	321	310	42	355	6.3	430	0.23
225	287	270	256	315	32	360	5.0	440	0.15
230	362	275	210	320	25	365	3.9	450	0.09

^aSource of data: DeMore and Tschuikow-Roux (1990); $\lambda > 360$ nm, Sander et al. (2006). The predominant photolytic process $\text{ClOOC1} + h\nu \rightarrow \text{Cl} + \text{ClOO}$ occurs with essentially unity quantum yield ($\phi_{\text{Cl}} \approx 1$)

Table 6.28 Absorption cross sections of hypochlorous acid, HOCl, at 298 K^a

λ (nm)	$10^{19} \sigma$ (cm ²)	λ (nm)	$10^{19} \sigma$ (cm ²)	λ (nm)	$10^{19} \sigma$ (cm ²)	λ (nm)	$10^{20} \sigma$ (cm ²)	λ (nm)	$10^{20} \sigma$ (cm ²)
200	0.72	245	1.94	290	0.513	335	2.81	380	0.708
205	0.56	250	1.73	295	0.561	340	2.22	385	0.602
210	0.55	255	1.40	300	0.600	345	1.76	390	0.491
215	0.71	260	1.09	305	0.612	350	1.43	395	0.384
220	1.02	265	0.821	310	0.597	355	1.20	400	0.288
225	1.39	270	0.625	315	0.555	360	1.06	405	0.182
230	1.75	275	0.510	320	0.495	365	0.968	410	0.144
235	1.99	280	0.464	325	0.424	370	0.888	415	0.097
240	2.07	285	0.473	330	0.350	375	0.804	420	0.063

^aSource of data: Burkholder (1993), Barnes et al. (1998). The dominant photolytic process is $\text{HOCl} + h\nu \rightarrow \text{OH} + \text{Cl}$ occurring with unity quantum yield at wavelengths $\lambda > 200$ nm (as reviewed by Sander et al. (2006))

Table 6.29 Absorption cross sections of chlorine, Cl₂, at 295 K^a

λ (nm)	$10^{20} \sigma$ (cm ²)	λ (nm)	$10^{20} \sigma$ (cm ²)	λ (nm)	$10^{20} \sigma$ (cm ²)	λ (nm)	$10^{20} \sigma$ (cm ²)	λ (nm)	$10^{21} \sigma$ (cm ²)
260	0.917	320	23.71	380	5.00	440	0.546	500	0.283
270	0.824	330	25.55	390	2.94	450	0.387	510	0.142
280	2.58	340	23.51	400	1.84	460	0.258	520	0.0681
290	6.22	350	18.77	410	1.28	470	0.162	530	0.0313
300	11.92	360	13.22	420	0.956	480	0.0957	540	0.0137
310	18.50	370	8.41	430	0.732	490	0.0534	550	0.0058

^aSource of data: Maric et al. (1993). The absorption band narrows somewhat with decreasing temperature. Photodissociation $\text{Cl}_2 + h\nu \rightarrow \text{Cl} (^2\text{P}_{3/2}) + \text{Cl} (^2\text{P}_{3/2})$ occurs with a quantum yield of unity

Table 6.30 Absorption cross sections of mixed halogen molecules BrCl, ICl, IBr^a

λ (nm)	$10^{19} \sigma$ ($\text{cm}^2 \text{ molecule}^{-1}$)			λ (nm)	$10^{19} \sigma$ ($\text{cm}^2 \text{ molecule}^{-1}$)			λ (nm)	$10^{20} \sigma$ ($\text{cm}^2 \text{ molecule}^{-1}$)		
	BrCl	ICl	IBr		BrCl	ICl	IBr		BrCl	ICl	IBr
280	0.0653	1.29	2.11	390	3.487	1.38	0.696	500	3.68	35.4	121.7
290	0.0357	0.64	1.68	400	2.895	1.90	1.20	510	2.59	29.0	115.9
300	0.0504	0.32	1.24	410	2.251	2.50	2.05	520	1.74	21.1	103.1
310	0.147	<0.1	0.795	420	1.780	2.85	3.17	530	1.13	15.6	85.8
320	0.408	<0.1	0.539	430	1.463	3.20	4.48	540	0.700	11.0	67.5
330	0.925	<0.1	0.336	440	1.255	3.54	5.87	550	0.419	7.3	52.3
340	1.721	<0.1	0.214	450	1.098	3.88	7.19	560	0.243	5.5	36.6
350	2.668	<0.1	0.145	460	0.952	4.17	8.52	570	0.136	4.2	27.2
360	3.503	0.23	0.152	470	0.802	4.20	9.85	580	0.074	3.4	19.9
370	3.961	0.46	0.237	480	0.647	4.18	11.11	590	0.039	2.9	14.6
380	3.926	0.874	0.417	490	0.499	4.00	11.99	600	0.020	2.1	11.3

^aSource of data: BrCl, Maric et al. (1994); ICl, Jenkin et al. (1990); IBr, Seery and Britton (1964)

Table 6.31 Absorption cross sections of bromine, Br₂, at 298 K^a

λ (nm)	$10^{21} \sigma$ (cm^2)		λ (nm)	$10^{20} \sigma$ (cm^2)		λ (nm)	$10^{20} \sigma$ (cm^2)		λ (nm)	$10^{20} \sigma$ (cm^2)	
	λ (nm)	σ (cm^2)		λ (nm)	σ (cm^2)		λ (nm)	σ (cm^2)		λ (nm)	σ (cm^2)
270	1.61	355	5.63	430	60.1	505	29.0	580	3.50		
280	0.728	360	8.66	435	57.1	510	26.2	585	2.98		
290	0.299	365	12.7	440	54.0	515	23.4	590	2.52		
295	0.187	370	17.8	445	51.2	520	20.6	595	2.11		
300	0.122	375	23.9	450	48.8	525	18.0	600	1.76		
305	0.100	380	30.7	455	46.8	530	15.7	605	1.45		
310	0.135	385	37.9	460	45.2	535	13.6	610	1.19		
315	0.274	390	45.1	465	44.0	540	11.7	615	0.958		
320	0.626	395	51.8	470	42.8	545	10.1	620	0.767		
325	1.41	400	57.4	475	41.6	550	8.68	625	0.607		
330	3.00	405	61.6	480	40.3	555	7.47	630	0.475		
335	6.02	410	64.2	485	38.6	560	6.43	635	0.368		
340	11.4	415	65.1	490	36.6	565	5.54	640	0.282		
345	20.5	420	64.5	495	34.3	570	4.77	645	0.214		
350	34.9	425	62.8	500	31.8	575	4.09	650	0.161		

^aSource of data: Maric et al. (1994); the spectrum consists of a broad continuum, with some overlapping band structure at wavelengths > 510 nm. A second, much weaker continuum occurs in the region 200–270 nm. Photodissociation $\text{Br}_2 + h\nu \rightarrow \text{Br} (^2\text{P}_{3/2}) + \text{Br} (^2\text{P}_{3/2})$ features a constant quantum yield in the range 480–680 nm, which is assumed to be unity. The formation of excited Br ($^2\text{P}_{1/2}$) atoms becomes possible – and has been observed – at wavelengths below 505 nm

Table 6.32 Absorption cross sections of iodine, I₂, at 295 K^a

λ (nm)	$10^{20} \sigma$ (cm ²)	λ (nm)	$10^{20} \sigma$ (cm ²)	λ (nm)	$10^{20} \sigma$ (cm ²)	λ (nm)	$10^{20} \sigma$ (cm ²)	λ (nm)	$10^{20} \sigma$ (cm ²)
210	418	310	18.1	410	4.43	510	277	610	40.8
220	302	320	12.2	420	5.96	520	309	620	30.5
230	225	330	7.79	430	13.5	530	326	630	28.0
240	169	340	4.71	440	20.3	540	306	640	23.6
250	128	350	2.58	450	33.3	550	265	650	21.6
260	97.1	360	1.24	460	57.1	560	191	660	19.0
270	72.9	370	0.659	470	89.7	570	130	670	17.7
280	54.4	380	1.14	480	131	580	92.7	680	14.9
290	38.9	390	0.925	490	179	590	65.8	690	12.8
300	27.4	400	2.93	500	228	600	47.4	700	10.3

^aAverages over 5 nm intervals; source of data: Saiz-Lopez et al. (2004). The absorption spectrum is continuous below 500 nm, pressure-dependent band structure occurs at longer wavelengths. The data were taken at sufficiently high bath gas pressures to approximate atmospheric conditions. Under these conditions, the quantum yield for photodissociation: I₂ + hν → I (²P_{3/2}) + I (²P_{3/2}) is unity. At wavelength below 530 nm a fraction of the iodine atoms is formed in the excited I (³P_{1/2}) state, which in the atmosphere are rapidly quenched by collisions

Table 6.33 Absorption cross sections of iodine nitrate, IONO₂, at 298 K^a

λ (nm)	$10^{18} \sigma$ (cm ²)	λ (nm)	$10^{18} \sigma$ (cm ²)	λ (nm)	$10^{18} \sigma$ (cm ²)	λ (nm)	$10^{18} \sigma$ (cm ²)	λ (nm)	$10^{18} \sigma$ (cm ²)
245	12.1	280	7.41	315	4.41	350	3.34	385	1.53
250	11.7	285	6.91	320	4.04	355	3.16	390	1.30
255	10.6	290	6.31	325	3.96	360	2.94	395	1.03
260	9.46	295	5.77	330	3.80	365	2.70	400	0.78
265	8.80	300	5.25	335	3.74	370	2.42	405	0.605
270	7.97	305	4.95	340	3.60	375	2.13	410	0.496
275	7.72	310	4.62	345	3.48	380	1.84	415	0.416

^aSource of data: Mössinger et al. (2002), cross sections represent 5 nm averages

Table 6.34 Absorption cross sections of bromine nitrate, BrONO₂, at 296 and 220 K^a

λ (nm)	$10^{19} \sigma$ (cm ²)		λ (nm)	$10^{19} \sigma$ (cm ²)		λ (nm)	$10^{20} \sigma$ (cm ²)		λ (nm)	$10^{21} \sigma$ (cm ²)	
	298 K	230 K		298 K	230 K		298 K	230 K		298 K	230 K
200	68.0	55.3	275	3.05	2.83	350	7.01	7.12	425	13.8	14.3
205	52.0	44.7	280	2.79	2.62	355	6.52	6.62	430	12.9	13.6
210	36.1	34.5	285	2.56	2.43	360	5.99	6.07	435	12.0	12.9
215	29.2	29.4	290	2.32	2.25	365	5.43	5.51	440	11.1	12.0
220	25.6	26.5	295	2.08	2.06	370	4.89	4.94	445	10.3	11.2
225	23.0	24.1	300	1.86	1.88	375	4.35	4.40	450	9.28	10.1
230	20.5	21.5	305	1.65	1.70	380	3.85	3.84	455	8.31	8.93
235	17.5	18.2	310	1.45	1.52	385	3.37	3.34	460	7.42	7.85
240	14.0	14.3	315	1.27	1.34	390	2.97	2.91	465	6.52	6.64
245	10.6	10.6	320	1.13	1.18	395	2.59	2.52	470	5.66	4.92
250	7.97	7.72	325	1.02	1.04	400	2.28	2.21	475	4.61	4.31
255	6.00	5.70	330	0.932	0.950	405	2.01	1.96	480	3.92	3.29
260	4.71	4.40	335	0.862	0.879	410	1.81	1.76	485	3.97	2.40
265	3.89	3.61	340	0.806	0.818	415	1.65	1.63	490	2.49	1.67
270	3.38	3.13	345	0.757	0.766	420	1.50	1.51	495	2.07	1.05

^aData source: Burkholder et al. (1995), Deters et al. (1998). At wavelength $\lambda > 300$ nm, the photodissociation process $\text{BrONO}_2 + h\nu \rightarrow \text{Br} + \text{NO}_3$ (ϕ_1) is dominant ($\phi_1 \approx 1$); at 248 nm ϕ_1 is reduced to $\phi_1 = 0.28$, indicating the occurrence of additional processes (Harwood et al. 1998)

Table 6.35 Absorption cross sections of hypobromous acid, HOBr, and hypoiodous acid, HOI^a

λ (nm)	$10^{20} \sigma$ (cm ²)		λ (nm)	$10^{20} \sigma$ (cm ²)		λ (nm)	$10^{20} \sigma$ (cm ²)		λ (nm)	$10^{21} \sigma$ (cm ²)	
	HOBr	HOI		HOBr	HOI		HOBr	HOI		HOBr	HOI
250	4.15		325	10.5	27.2	400	2.43	32.2	475	16.2	5.25
255	6.19		330	10.8	32.9	405	1.80	33.2	480	13.0	2.96
260	10.5		335	11.3	37.0	410	1.36	32.7	485	9.93	1.61
265	14.6		340	11.9	38.5	415	1.08	30.7	490	7.23	0.86
270	18.7		345	12.3	37.7	420	0.967	27.5	495	5.02	
275	22.1		350	12.4	34.7	425	0.998	23.5	500	3.33	
280	24.3	0.077	355	12.1	30.4	430	1.15	19.2	505	2.12	
285	25.0	0.226	360	11.5	25.8	435	1.40	15.0	510	1.29	
290	24.0	0.589	365	10.5	22.1	440	1.68	11.3	515	0.76	
295	21.9	1.37	370	9.32	19.8	445	1.96	8.13	520	0.42	
300	19.1	2.86	375	7.99	19.4	450	2.18	5.63	525	0.23	
305	16.2	5.41	380	6.65	20.7	455	2.29	3.76	530	0.12	
310	13.6	9.26	385	5.38	23.3	460	2.28	2.42	535	0.059	
315	11.8	14.5	390	4.22	26.6	465	2.14	1.50	540	0.029	
320	10.8	20.7	395	3.23	29.8	470	1.91	0.904	545	0.013	

^aSource of data: HOBr (298 K) Ingham et al. (1998); HOI (295 K) Bauer et al. (1998)

Quantum yields:

1. The photodissociation process $\text{HOBr} + h\nu \rightarrow \text{Br} + \text{OH}$ (φ_1) is expected to occur with unity quantum yield ($\varphi_1 \approx 1$), similar to photodissociation of HOCl.
2. The process $\text{HOI} + h\nu \rightarrow \text{I} + \text{OH}$ (φ_2) has been found to occur with a quantum yield $\varphi_2 = 1$ at 355 nm (Bauer et al. (1998), which may be assumed to apply to the entire wavelength region.

References

- Anderson, S.M., P. Hupalo, K. Mauersberger, *Geophys. Res. Lett.* **20**, 1579–1582 (1993)
- Atkinson, R., D.L. Baulch, R.A. Cox, J.N. Crowley, R.F. Hampson Jr., R.G. Hynes, M.E. Jenkin, M.J. Rossi, J. Troe, *Atmos. Chem. Phys.* **4**, 1461–1738 (2004)
- Atkinson, R., D.L. Baulch, R.A. Cox, J.N. Crowley, R.F. Hampson Jr., R.G. Hynes, M.E. Jenkin, M.J. Rossi, J. Troe, *Atmos. Chem. Phys.* **6**, 3625–4055 (2006)
- Atkinson, R., D.L. Baulch, R.A. Cox, J.N. Crowley, R.F. Hampson Jr., R.G. Hynes, M.E. Jenkin, M.J. Rossi, J. Troe, *Atmos. Chem. Phys.* **7**, 981–1191 (2007)
- Barnes, R.J., A. Sinha, H.A. Michelsen, *J. Phys. Chem. A* **102**, 8855–8859 (1998)
- Bauer, D., T. Ingham, S.A. Carl, G.K. Moortgat, J.N. Crowley, *J. Phys. Chem. A* **102**, 2857–2864 (1998)
- Blitz, M.A., D.E. Heard, M.J. Pilling, S.R. Arnold, M.P. Chipperfield, *Geophys. Res. Lett.* **31**, L06111, 1–5 (2004). doi:10.1029/2003GL018793
- Brion, J., A. Chakir, J. Charbonnier, D. Daumont, C. Parisse, J. Malicet, *J. Atmos. Chem.* **30**, 29–299 (1998)
- Burkholder, J.B., *J. Geophys. Res.* **98**, 2963–2974 (1993)
- Burkholder, J.B., R.K. Talukdar, A.R. Ravishankara, *Geophys. Res. Lett.* **21**, 585–588 (1994)
- Burkholder, J.B., A.R. Ravishankara, S. Solomon, *J. Geophys. Res.* **100**, 16793–16800 (1995)
- Cacciani, M., A. di Sarra, G. Fiocco, A.A. Amuroso, *J. Geophys. Res.* **94**, 8485–8490 (1989)
- DeMore, W.B., E. Tschuikow-Roux, *J. Phys. Chem.* **94**, 5856–5860 (1990)
- Deters, B., J.P. Burrows, J. Orphal, *J. Geophys. Res.* **103**, 3563–3570 (1998)
- Gierczak, T., J.B. Burkholder, S. Bauerle, A.R. Ravishankara, *Chem. Phys.* **231**, 229–244 (1998)
- Harwood, M.H., R.L. Jones, R.A. Cox, E. Lutman, O.V. Rattigan, *J. Photochem. Photobiol. A* **73**, 167–175 (1993)
- Harwood, M.H., J.B. Burkholder, A.R. Ravishankara, *J. Chem. Phys. A* **102**, 1309–1317 (1998)
- Hubrich, C., F. Stuhl, *J. Photochem.* **12**, 93–107 (1980)
- Ingham, T., D. Bauer, J. Landgraf, J.N. Crowley, *J. Chem. Phys. A* **104**, 3293–3298 (1998)
- Jenkin, M.E., R.A. Cox, A. Mellouki, G. Le Bras, G. Poulet, *J. Phys. Chem.* **94**, 2927–2934 (1990)
- Jenouvrier, A., B. Coquart, M.F. Mérienne, *J. Atmos. Chem.* **25**, 21–32 (1996)
- Jimenez, E., T. Gierczak, H. Stark, J.B. Burkholder, A.R. Ravishankara, *Phys. Chem. Chem. Phys.* **7**, 342–348 (2005)
- Johnston, H.S., H.F. Davis, Y.T. Lee, *J. Phys. Chem.* **100**, 4713–4723 (1996)
- Kang, W.K., K. Jung, D.-C. Kim, K.-H. Jung, *J. Chem. Phys.* **104**, 5815–5820 (1996)
- Keller-Rudek, H., G.K. Moortgat, *MPI-Mainz-UV-VIS-Spectral-Atlas of Gaseous Molecules* (2010). www.atmosphere.mpg.de/spectral-atlas-mainz
- Malicet, J., D. Daumont, J. Charbonnier, C. Parisse, A. Chakir, J. Brion, *J. Atmos. Chem.* **21**, 263–273 (1995)
- Maric, D., J.P. Burrows, R. Meller, G.K. Moortgat, *J. Photochem. Photobiol. A* **70**, 205–214 (1993)

- Maric, D., J.P. Burrows, G.K. Moortgat, J. Photochem. Photobiol. A **83**, 179–192 (1994)
- Martinez, R.D., A.A. Buitrago, N.W. Howell, C.H. Hearn, J.A. Joens, Atmos. Environ. **26A**, 685–792 (1992)
- Matsumi, Y., F.J. Comes, G. Hancock, A. Hofzumahaus, A.J. Hynes, M. Kawasaki, A.R. Ravishankara, J. Geophys. Res. **107**, D3 4124, (2002). doi:10.1029/2001JD000510
- Meller, R.E., G.K. Moortgat, J. Geophys. Res. **105**, 7089–7101 (2000)
- Mérienne, M.F., B. Coquart, A. Jenouvrier, Planet. Space Sci. **38**, 617–625 (1990)
- Mérienne, M.F., A. Jenouvrier, B. Coquart, J. Atmos. Chem. **20**, 281–297 (1995)
- Molina, L.T., M.J. Molina, J. Geophys. Res. **91**, 14501–14508 (1986)
- Molina, L.T., J.J. Lamb, M.J. Molina, Geophys. Res. Lett. **8**, 1008–1011 (1981)
- Moortgat, G.K., W. Seiler, P. Warneck, J. Chem. Phys. **78**, 1185–1190 (1983)
- Moortgat, G.K., H. Meyrahn, P. Warneck, Chem. Phys. Chem. **11**, 3896–3908 (2010)
- Mössinger, J.C., D.M. Rowley, R.A. Cox, Atmos. Chem. Phys. **2**, 227–234 (2002)
- Nan, G., I. Burak, P.L. Houston, Chem. Phys. Lett. **209**, 383–389 (1993)
- Ogorzalek, L.R., H.-P. Haerri, G.E. Hall, P.L. Houston, J. Chem. Phys. **90**, 4222–4236 (1989)
- Orphal, J.S., E. Fellows, J.-M. Flaud, J. Geophys. Res. **108**, 4077 (2003). doi: 10.1029/2002JD002489
- Osborne, B.A., G. Marston, L. Kaminski, N.C. Jones, J.M. Gingell, N. Mason, I.C. Walker, J. Delwiche, M.-J. Hubin-Franskin, J. Quant. Spectros. Radiat. Transfer **64**, 67–74 (2000)
- Rattigan, O.V., D.E. Shallcross, R.A. Cox, J. Chem. Soc. Faraday Trans. **93**, 2839–2846 (1997)
- Rebert, R.E., P. Ausloos, J. Photochem. **4**, 419–434 (1975)
- Rebert, R.E., P. Ausloos, J. Photochem. **6**, 265–276 (1977)
- Saiz-Lopez, A., R.W. Saunders, D.M. Joseph, S.H. Ashworth, J.M.C. Plane, Atmos. Chem. Phys. **4**, 1443–1450 (2004)
- Sander, S.P., J. Phys. Chem. **90**, 4135–4142 (1986)
- Sander, S.P., R.R. Friedl, D.M. Golden, M.J. Kurylo, G.K. Moortgat, H. Keller-Rudek, P.H. Wine, A.R. Ravishankara, C.E. Kolb, M.J. Molina, B.J. Finlayson-Pitts, R.E. Huie, V.L. Orkin, NASA Chemical Kinetics and Photochemical Data for Use in Atmospheric Studies, Evaluation Number 15, JPL Publication 06–2 (Jet Propulsion Laboratory, California Institute of Technology, Pasadena, 2006)
- Seery, D.J., D. Britton, J. Phys. Chem. **68**, 2263–2266 (1964)
- Selwyn, G., J. Podolske, H.S. Johnston, Geophys. Res. Lett. **4**, 427–430 (1977)
- Simon, P.C., D. Gillotay, N. Vanlaethem-Meuree, J. Wisenberg, J. Atmos. Chem. **7**, 107–135 (1988)
- Stutz, J., E.S. Kim, U. Platt, P. Bruno, C. Perrino, A. Febo, J. Geophys. Res. **105**, 14585–14592 (2000)
- Talukdar, R.K., C.A. Longfellow, M.K. Gilles, A.R. Ravishankara, Geophys. Res. Lett. **25**, 143–146 (1998)
- Troe, J., Z. Phys. Chem. **214**, 573–581 (2000)
- Uma, S., P.K. Das, Can J. Chem. **72**, 865–869 (1994)
- Vandaele, A.C., C. Hermans, P.C. Simon, M. Carleer, R. Colin, S. Fally, M.F. Merienne, A. Jenouvrier, B. Coquart, J. Quant. Spectros. Radiat. Transfer **59**, 171–184 (1998)
- Warneck, P., Atmos. Environ. **35**, 5773–5777 (2001)
- Yao, F., I. Wilson, H. Johnston, J. Phys. Chem. **86**, 3611–3615 (1982)
- Yoshino, K., A.S.C. Cheung, J.R. Esmond, W.H. Parkinson, D.E. Freeman, S.L. Guberman, A. Jenouvrier, B. Coquart, M.F. Merienne, Planet. Space Sci. **36**, 1469–1475 (1988)
- Yoshino, K., J.R. Esmond, A.S.C. Cheung, D.E. Freeman, W.H. Parkinson, Planet. Space Sci. **40**, 185–192 (1992)
- Zhao, Z., R.E. Stickel, P.H. Wine, Geophys. Res. Lett. **22**, 615–618 (1995)